Int J Adv Manuf Technol (2017) 90:605–634
DOI 10.1007/s00170-016-9225-9

ORIGINAL ARTICLE

A review on resistance spot welding of aluminum alloys

S. M. Manladan[1,2] · F. Yusof[1,3] · S. Ramesh[1,3] · M. Fadzil[3] · Z. Luo[4,5] · S. Ao[4]

Received: 3 May 2016 / Accepted: 25 July 2016 / Published online: 5 September 2016

Abstract This paper presents a review on the resistance spot welding (RSW) of Al/Al alloys, Al alloys/steel, Al/Mg alloys, and Al/Ti alloys, with focus on structure, properties, and performance relationships. It also includes weld bonding, effect of welding parameters on joint quality, main metallurgical defects in Al spot welds, and electrode degradation. The high contact resistance, induced by the presence of oxide layer on the surface of Al alloys, and the need for application of high welding current during RSW of Al alloys result in rapid electrode tip wear and inconsistency in weld quality. Studies have shown that cleaning the oxide layer, sliding of a few microns between sheets, enhancing the electrode force, and the application of a low-current pre-heating can significantly reduce the contact resistance and improve joint quality. For Al/steel dissimilar RSW, the technique of resistance element welding, the use of optimized electrode morphology, the technique of RSW with cover plates, and the use of interlayers such as Al-Mg, AlSi12, and AlCu28 alloys were found to suppress the formation of brittle intermetallic compounds (IMC) and improve the joint quality. The employment of pure Ni foil, Au-coated Ni foil, Sn-coated steel, and Zn-coated steel interlayers was also found to restrict the formation of brittle IMCs during RSW of Al/Mg alloys. Furthermore, the techniques of RSW with cover plates and RSW under the influence of electromagnetic stirring effect were found to improve the weldability of Al/Ti dissimilar alloys.

Keywords Resistance spot welding · Aluminum alloys · Magnesium alloys · Titanium alloys · Microstructure · Intermetallic compounds · Failure mode · Weld bonding · Metallurgical defects · Electrode degradation · Welding parameters

✉ F. Yusof
farazila@um.edu.my

S. M. Manladan
smmanladan.mec@buk.edu.ng

S. Ramesh
ramesh79@um.edu.my

M. Fadzil
ibnjamaludin@um.edu.my

Z. Luo
lz@tj.edu.cn

S. Ao
aosanmick@163.com

[1] Department of Mechanical Engineering, Faculty of Engineering, University of Malaya, 50603 Kuala Lumpur, Malaysia

[2] Department of Mechanical Engineering, Faculty of Engineering, Bayero University, Kano, 3011 Kano, Nigeria

[3] Center for Advanced Manufacturing and Materials Processing (AMMP), Faculty of Engineering, University of Malaya, 50603 Kuala Lumpur, Malaysia

[4] School of Materials Science and Engineering, Tianjin University, Tianjin 300072, China

[5] Collaborative Innovation Center of Advanced Ship and Deep-Sea Exploration, Shanghai 200240, China

1 Introduction

Fossil fuel combustion is one of the largest sources of anthropogenic greenhouse gas emission [1, 2]. Thus, the transportation industry, the largest consumer of fossil fuel, is continuously exploring strategies to improve fuel efficiency and reduce greenhouse gas emission. These strategies include weight reduction, improving conventional engine efficiency, developing new and more energy efficient powertrains, such

as electric and hybrid systems, and the use of low CO_2 fuels, such as biofuels [3, 4]. Of these strategies, weight reduction has been identified as the most cost-effective. On the average, for a vehicle, a weight reduction of 100 kg could lead to a fuel saving of about 0.5 L per 100 km [5, 6] and a reduction of 9 g of CO_2 per km [7]. Generally, for every 10 % weight reduction, the specific fuel consumption could reduce by 3–7 %, while maintaining the same functionality [1–3]. Thus, lightweight materials are increasingly being developed and incorporated into automotive and aerospace structures [4, 8].

Owing to their low density, approximately one third that of steel, and high strength and stiffness to weight ratio, Al alloys have great potentials for weight reduction. In most applications, they allow a weight saving of up to 50 % over conventional materials without compromising strength and safety. Al alloys also possess excellent corrosion resistance, low-energy formability, good crashworthiness, high thermal and electrical conductivities, high reflectivity to both heat radiation and light, good machinability, and mass production capabilities at a reasonable price [7, 9–17]. Furthermore, they have excellent recyclability, and low secondary energy cost, which enables the Al industry to recycle all available scrap with only about 5 % of the energy required to produce new Al alloys. Thus, Al alloys attract tremendous attention in aerospace, naval, automotive, and other industries, in a variety of product forms—sheet, casting, and extrusion. Some applications of Al in vehicles include in body panels, power trains, closures, chassis, brake housings, air deflector parts, and seat slides [18–22]. In the future, they are expected to replace steel as the primary construction material in the automotive industry [7, 10, 23–27]. For a North American light duty vehicle, for instance, there is a projected increase in net Al content from 394 lb per vehicle in 2015 to about 547 lb per vehicle in 2025 [28].

RSW is the most widely used sheet joining process, especially in the automotive industry, because of advantages such as low-cost, reliability, high speed, ease of operation and automation, and suitability for use in high-volume production [26, 29–32]. There are approximately 5000 spot welds in a single automobile [33–36]. The quality, structural performance, lifespan, safety design, strength, stiffness, and integrity of a vehicle depend not only on the mechanical properties of the sheets but also on the quality of spot welds. Furthermore, the vehicle crashworthiness, which is defined as the capability of a car structure to provide adequate protection to its passengers against injuries in the event of a crash, largely depends on the integrity and the mechanical performance of spot welds [35, 37, 38].

Recently, there is an increased interest in high-volume RSW of Al alloys [13, 14, 16, 25]. However, unlike the RSW of steel, which readily produces high-quality and durable welds [39], the RSW of Al alloys present some difficulties. Al alloys possess lower bulk resistance and higher thermal and electrical conductivities than steel, necessitating the use of high welding currents, typically two to three times higher than that required for steel. Moreover, the presence of an oxide layer on the surface of Al alloys induces high contact resistance and heat development. These lead to rapid electrode tip degradation and inconsistency in joint quality [16, 31, 40–44]. Furthermore, the RSW of Al alloys is more sensitive to abnormal process conditions, such as axial misalignment, angular misalignment, and poor fit-up, than that of steel [24, 45]. Therefore, the growing interest in high-volume RSW of Al alloys is accompanied with a challenge to better understand and improve the process, structure, properties, and performance relationships. This paper reviews the RSW of Al/Al alloys, Al alloys/steel, Al/Mg alloys, and Al/Ti alloys, with emphasis on structure, properties, and performance relationships, under quasi-static and dynamic loading conditions. The aim of the paper is to provide an account of the state of understanding of RSW of Al alloys, with a view to providing a basis for subsequent research.

2 Fundamentals of resistance spot welding

As illustrated in Fig. 1, RSW process typically involves placing two or more overlapping metal sheets between two water-cooled electrodes and then applying pressure onto the electrodes in order to clamp the workpieces together and also produce close contact between them. Thereafter, electrical current is supplied to the workpieces via the two electrodes for a specific period of time. The resistance of the sheets to the flow of a localized electrical current results in heat generation, and consequently a molten nugget is formed at the faying

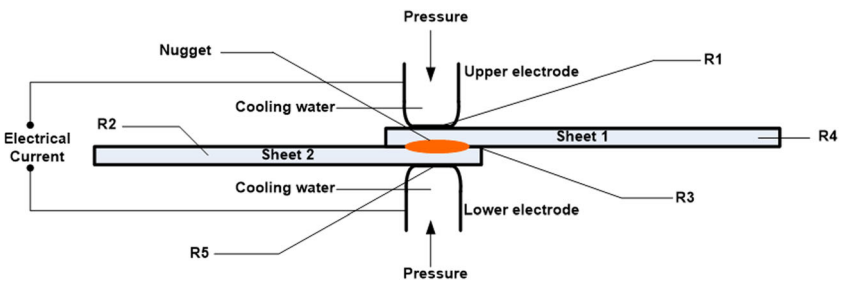

Fig. 1 Illustration of the principles of RSW

interface. The current is finally switched off while the electrode pressure is maintained and thus the nugget begins to cool and solidify. The cooling is facilitated by heat conduction through the two water-cooled electrodes and radially outwards through the sheets [46–49].

Heat generation in RSW is based on Joule's law, which is expressed as follows [50]:

$$Q = I^2Rt \quad (1)$$

where Q is heat input in joules, I is the current in amperes, R is the resistance in ohms, and t is the time in seconds. Thus, the quantity of heat generated depends on the current, resistance, and duration of application of welding current [35].

As depicted in Fig. 1, there are two kinds of resistances in RSW process, i.e., contact resistance, which exists at the electrode/sheet interfaces (R1 and R5) and at the faying interface (R3), and bulk resistance (R2 and R4) [51]. In addition to these, the resistances of the upper electrode (R_U) and that of the lower electrode (R_L) also contribute to the total resistance, which is the sum of all the resistances ($R_U + R1 + R2 + R3 + R4 + R5 + R_L$) [52]. Of all these resistances, R3 is the most significant since the nugget formation initiates here. If it is too low, there will be insufficient heat generation to achieve nugget formation. On the other hand, if it is too high, there will be excessive heat generation [52–54].

3 Surface characteristics and contact resistance

The surface characteristics of Al alloys strongly influence the RSW process, weld quality, and electrode degradation. The most influential surface characteristics are the presence of an oxide layer, surface roughness, and the presence of a chemical or lubricant [42, 55–57].

Due to its high affinity for oxygen, a tough, non-conducting, adherent, and refractory Al oxide film (Al_2O_3) forms on the surface of Al alloys. Although this oxide layer gives corrosion protection, it induces high contact resistance at both the electrode/workpiece and faying interfaces, leading to severe electrode degradation and scatter in weld quality. The extent of these problems depends on the thickness of the oxide layer [25, 42, 55, 58–60]. Thus, to facilitate RSW of Al alloys, the oxide layer needs to be cleaned or reduced [36, 56–58]. The cleaning can be done mechanically, using abrasive papers [14, 27, 42, 58, 61–67] or chemically using, for example, NaOH solution [68, 69]. Full cleaning of the oxide layer results in better weld quality than reduced cleaning (incomplete removal) [56]. For example, under identical welding conditions, samples of AA5754 Al alloy subjected to full cleaning exhibited better weld quality, wider process window, and a lower tendency to electrode sticking than those subjected to reduced cleaning [56].

Apart from cleaning, enhanced electrode force was found to be beneficial in squeezing and breaking down the oxide film and thus reducing the contact resistance [25, 44, 54]. Furthermore, it has been reported that a small relative rotation or sliding of a few microns between sheets could result in large reduction in contact resistance [53, 54]. For instance, a relative rotation of only 1° under the axial force of 1 kN was sufficient to reduce the contact resistance at the faying surface of coated 5754 Al alloy from 7000 to 110 μΩ [53]. However, this method is difficult to implement in high-volume production in industrial setting due to the fixation of the assembled panels in given positions [25]. Therefore, Luo et al. [25] proposed the application of a low-current pre-heating treatment to suppress the effect of oxide layer. As shown in Fig. 2, a pre-heating current of 8 kA for a pre-heating time of 50 ms resulted in significant reduction in contact resistance at the faying interface of AA5052 Al alloys and also improved its distribution. Consequently, the joint quality and consistency improved significantly [25].

Furthermore, lubricants, which are applied in body panel stamping process to improve formability, were also found to significantly increase contact resistance and risk of expulsion during RSW of Al alloys. However, it was observed that introducing a low-current pre-pulse into the welding schedule could displace the lubricant and thus reduce the risk of expulsion [56].

4 Nugget formation during RSW of Al alloys

The nugget formation process in RSW of Al alloys has been studied using experimental investigation and numerical simulation [55, 70, 71]. The studies have shown that, in the electrode squeezing process, several cracks form in the surface oxide layer in the entire contact zone of the faying surfaces, with more cracks forming at the periphery than at the center of

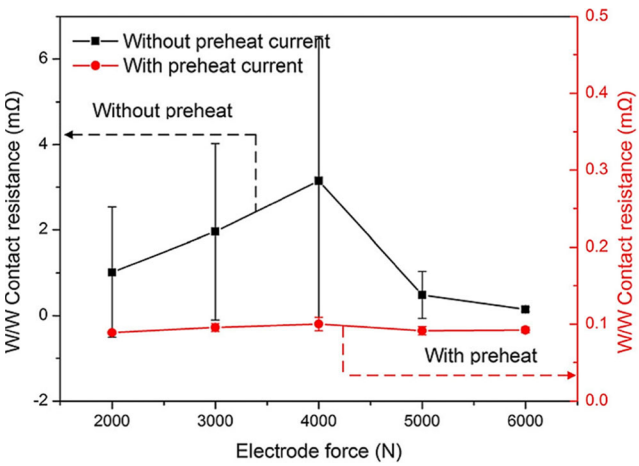

Fig. 2 The effect of pre-heating on the contact resistance at the faying surface of AA5052 Al alloys (pre-heating current of 8 kA, pre-heating time of 50 ms) [25]

the contact zone due to sheet separation. The cracks from both sheets tend to align with each other at the periphery to form larger cracks and hence greater metal-to-metal contacts [55]. Thus, the periphery of the contact zone provides the preferred current flow path. Consequently, at the beginning of nugget formation, melting starts in a ring near the periphery, forming two liquid nuggets, as shown in Fig. 3. With increased welding time, the melting proceeds rapidly inwards from all directions and the two nuggets merge to produce a complete nugget [55, 70]. Faster growth rate was observed for the first cycle after which the nugget expansion occurred gradually due to the drop in electrical contact resistance [55]. A study of the nugget formation during RSW of 5052 Al alloy in three-sheet configuration has shown that at the initial stage, two small nuggets formed simultaneously at both the upper and lower workpiece/workpiece interfaces. As the welding time increased, the two small nuggets grew along the radial and axial directions and then fused into one I-shaped nugget, as shown in Fig. 4. The nugget grew larger and eventually became elliptical in shape, with the maximum nugget diameter located at the center of the middle sheet. The nugget diameter at the upper interface was always larger than that at the lower interface. This was attributed to Peltier effect between the copper electrode and Al alloy. With the upper electrode as positive, heat is generated at the upper electrode/workpiece (i.e., Cu-Al) interface, while heat is absorbed at the lower electrode/sheet interface (i.e., Al-Cu). This resulted in higher heat generation and slightly larger nugget size at the upper interface [71]

5 Microstructure

The microstructure of a weld is determined by the composition of the base alloy and its thermal history [51]. It is also controlled by a combination of the prevailing thermal condition at the solid/liquid interface and the rate of growth of crystals, which is directly related to the thermal gradient in the weld [72].

Generally, the microstructure of Al alloy resistance spot welds can be divided into three distinct zones: the base metal (BM), the heat-affected zone (HAZ), and the fusion zone (FZ) or nugget zone [19, 63, 73]. Furthermore, characterization of the microstructure of resistance spot welds of AA 6061-T6 [73], AA6111-T4 [19], 6082-T6 [63], 5083-O [22], AA5052 [30, 71], and 7075 [21] Al alloys has shown that the FZ contained two different microstructures, i.e., a columnar grain structure at the edge of the nugget and an equiaxed grain structure in the nugget center. The reason for the two different microstructures could be associated with the variation in cooling rate within the nugget zone [19, 73]. A study of the microstructural evolution during RSW of three-sheet AA5052 Alloy has shown that, at a short welding time of 50 ms, when

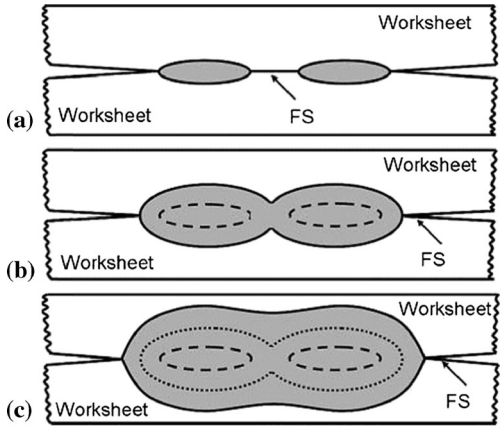

Fig. 3 Nugget formation model during RSW of AA5182 Al alloy. **a** Start of heating at periphery; **b** heating grows more rapidly inwards than outwards; **c** completion of nugget formation [55]

two nuggets were observed (one at each interface), a very thin columnar crystal zone was observed at the edge of each nugget (Fig. 5b) while an equiaxed crystal zone, consisting of equiaxed α-Al grains and β-Al_3Mg_2 phases, was observed at the interior of the nugget, as shown in Fig. 5d. Furthermore, a partially melted zone (PMZ) was observed between the two nuggets (Fig. 5c). At 200 ms, when the nugget formation was completed, a cellular dendritic zone was also observed at the edge of the nugget due to higher peak temperature [71]

The columnar-to-equiaxed transition (CET) occurs when the movement of the columnar front is blocked by the formation of enough equiaxed grains in the liquid ahead of the columnar front. Compared to the columnar dendritic structure, the equiaxed grains are finer, have more isotropic structure and less segregation of alloying elements, and have better mechanical properties. It is therefore important to promote the formation of equiaxed grains [74–76]. Li et al. [30, 68] found that RSW of Al alloys under the influence of electromagnetic stirring (EMS) effect, produced by mounting two identical permanent magnets coaxially on the electrode arms with opposite polarities, leads to microstructure refinement and promotes CET. The EMS would drive the high temperature molten metal, in a centrifugal motion, from the center of the nugget to its edge, thereby lowering the temperature gradient in the liquid nugget. Moreover, the EMS would break the growing columnar dendrites during the primary crystallization process. These would constrain the growth of columnar dendrites and thus promote CET [30, 68].

Figure 6 compares the microstructure of 6061-T6 Al alloy resistance spot welds produced with and without EMS [68]. As shown in the figure, for both cases, a partially melted zone (PMZ) was observed at the edge of the nugget and a columnar grain zone (CGZ) next to it. Furthermore, a transition zone was found to connect the CGZ and the equiaxed grain zone

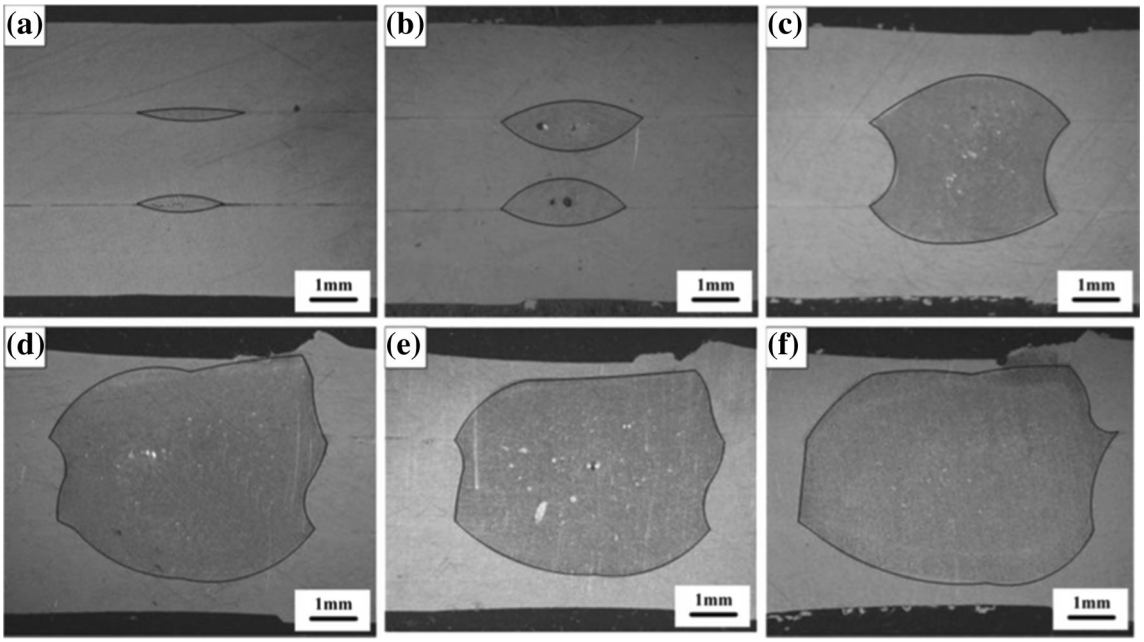

Fig. 4 Nugget formation in three-sheet A5052 Al alloy RSW at **a** 40 ms, **b** 50 ms, **c** 100 ms, **d** 150 ms, **e** 200 ms, and **f** 350 ms [71]

(EGZ). Under the EMS, the microstructures in all the zones of the joint are refined. The CGZ and transition zone are narrower. However, the PMZ is larger with EMS. The movement of the high temperature molten metal to the edge of the nugget by EMS has led to more heating at the edge of the nugget, and as a result, the size of the PMZ increased [68].

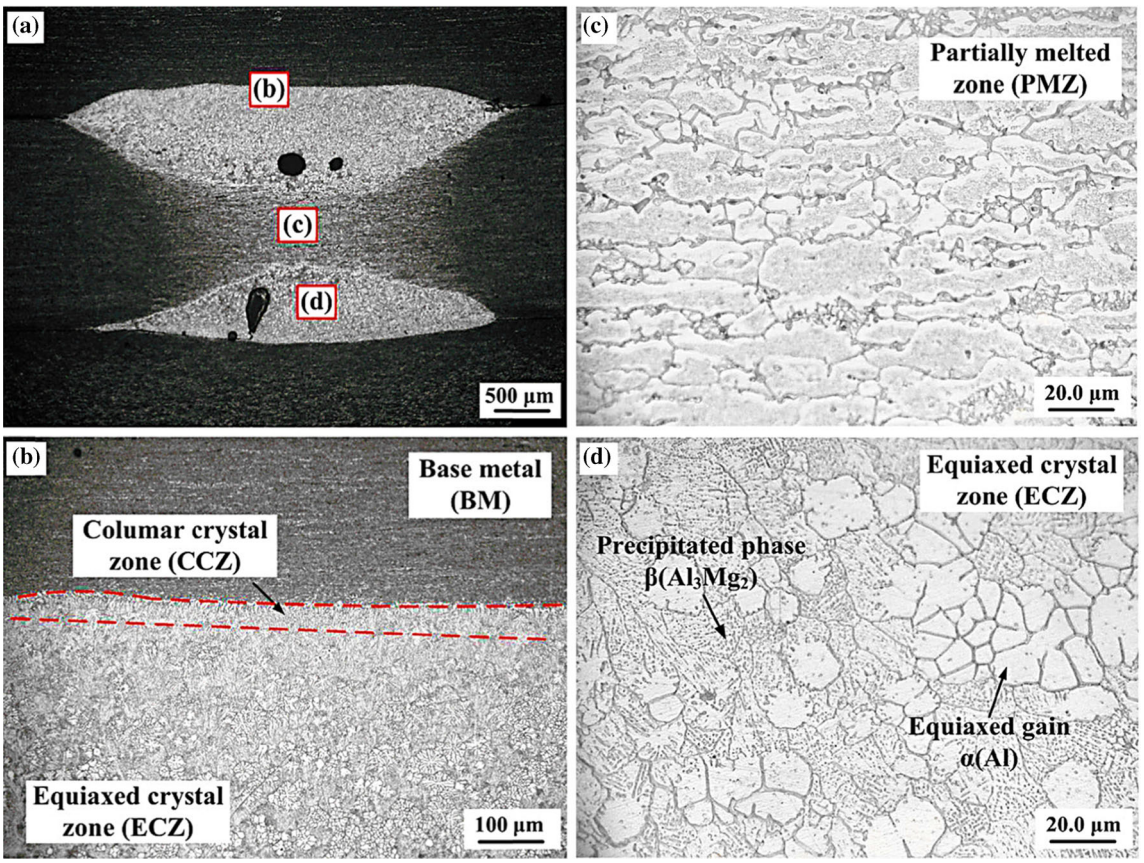

Fig. 5 Microstructure of three-sheet AA5052 Al alloy weld at a welding time of 50 ms **a**) morphology of regions magnified in b-d; microstructure of **b**) region b in a, **c**) region c in a, **d**) region d in a

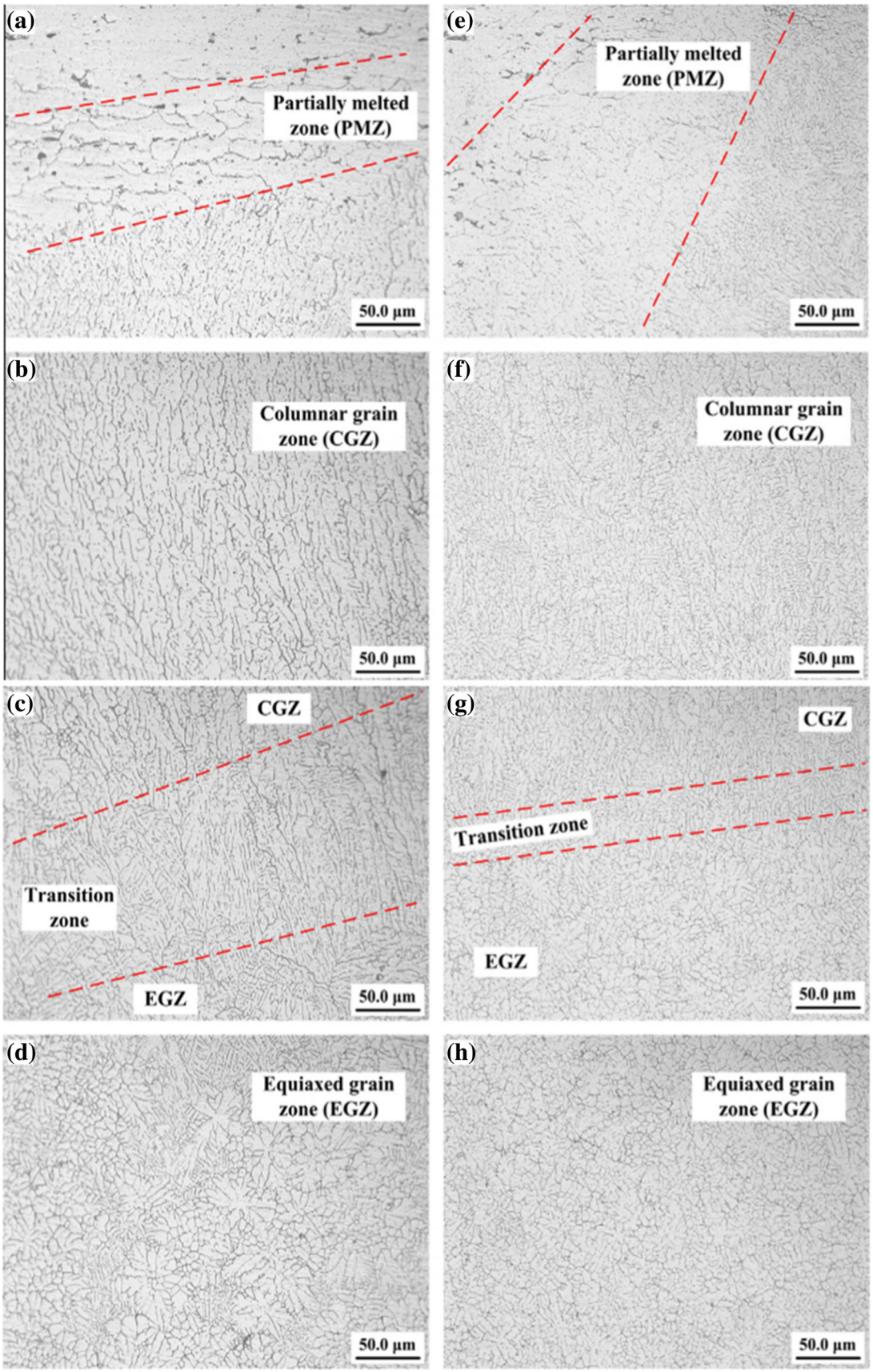

Fig. 6 Microstructure of 6061-T6 Al alloy resistance spot weld: **a**–**d** conventional RSW; **e**–**h** RSW with EMS [68]

The HAZ is characterized by recrystallization and grain growth [19, 27, 41, 73]. Figure 7 shows the electron backscatter diffraction (EBSD) mapping of the grain size and orientation due to the recrystallization process for 6061-T6 Al alloy resistance spot weld. The grain size in the FZ, HAZ, and BM was found to be 10.63, 22.90, and 16.62 μm, respectively. The reduction of grain size in the FZ is due to the high cooling rate during solidification, as opposed to the residual heat experienced in the HAZ, which has led to grain growth [27, 41]. In another study, a thin zone, with large and coarse grains, was observed in the area between nugget and HAZ of 6061-T6 Al alloy due to the attainment of extremely high temperature. However, beyond this zone, the HAZ consists of very small and fine grains [73]. Furthermore, a small amount of grain growth was observed in the HAZ, close to the nugget of AA6111-T4 Al alloy. Minor amount of grain boundary melting and re-solidification occurred, leading to inter-grain dendritic growth. However, most grains in the HAZ had the same size as those in the BM [19].

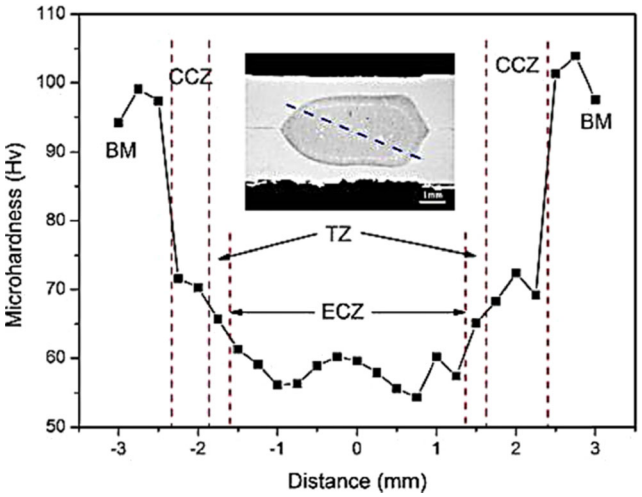

Fig. 8 Hardness profile of 6061-T6 Al alloy resistance spot weld [69]

6 Mechanical properties

6.1 Hardness

Generally, a significant reduction in hardness has been observed in the HAZ and FZ of resistance spot welds of heat treatable, 6xxx series Al alloys [18, 19, 63, 73, 77]. This is attributed to the dissolution of strengthening precipitates, especially in the T6 state [18, 63, 73] and to the destruction of work hardening [19]. Figure 8 shows the hardness profile across the BM, columnar crystal zone (CCZ), transition zone (TZ), and equiaxed crystal zone (ECZ) of 6061-T6 Al alloy resistance spot weld. As shown in the figure, the decrease in hardness is concentrated mainly in the nugget, where the melting of the BM has led to the total dissolution of the strengthening precipitates [18, 63, 78]. A similar observation was made for 6082-T6 [63], AA6111-T4 [19], and AA6022-T4 [77] Al alloys resistance spot welds. For 6061-T6 Al alloy, the average microhardness value of the BM, CGZ, TZ, and EGZ was found to be 96, 70, 64, and 59 HV, respectively. It was found that under EMS, the average hardness of EGZ increased from 59 HV to about 64 HV, due to microstructure refinement [68]. For AA6111-T4 Al alloy, the nugget center was found to be approximately 35 % softer than the sheet surface [19].

Unlike in heat treatable, 6xxx series Al alloys, where there is significant reduction in hardness of the FZ, minimal variation in hardness has been reported for non-heat treatable, 5xxx series Al alloys spot welds [18]. Figure 9 compares the hardness profile of AA5754 and AA6111-T4 Al alloy resistance spot welds. As shown, the average hardness value of AA6111 Al alloy BM is significantly higher than that of AA5754 Al alloy. However, the hardness value of the FZ of AA6111 Al alloy experienced a significant reduction to a value below that

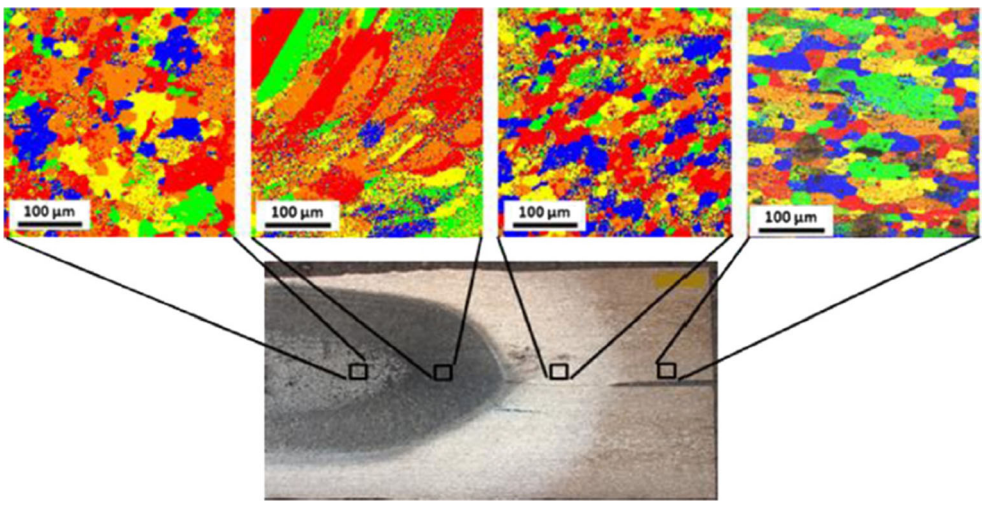

Fig. 7 EBSD mapping of the grain size and orientation in 6061-T6 Al alloy resistance spot weld [41]

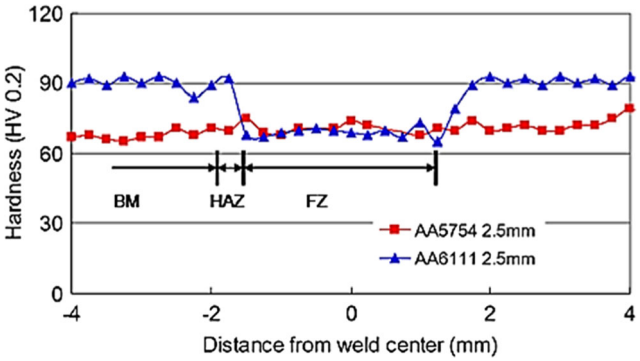

Fig. 9 Comparison of the hardness profiles of AA5754 and AA6111 Al alloys [18]

of AA5754 Al alloy because melting and re-solidification has led to the removal of precipitation hardening which existed in the BM [18]

A comparison of the microhardness values of AA5052 Al alloy spot welds, produced with and without EMS (Fig. 10), has shown that both welds had similar hardness values at the center of the nugget. However, the CGZ of the joint made with EMS exhibited higher hardness value due to columnar refinement (the grain size of the CGZ with and without EMS was found to be 9.3 and 16.7 μm, respectively). Furthermore, as shown in Fig. 10, the HAZ of the joint with EMS was softer, implying improved ductility [30].

6.2 Strength and failure mode

The mechanical performance of spot welds is normally studied under quasi-static and dynamic loading conditions. The tests that are conducted under quasi-static loading conditions include tensile shear (TS), cross-tension (CT), and coach peel (CP) tests. Impact and fatigue tests are some of the tests conducted under dynamic loading conditions [37]. Tensile shear is the most widely used test because of the simplicity in samples preparation [79]. The load-bearing capacity (peak load) and energy absorption are extracted from the load-displacement curve obtained from the test [37]. Failure mode of spot welds is a qualitative measure of mechanical performance and an indicator of their load-bearing and energy absorption capacities [37]. Spot welds commonly fail in three distinct modes, i.e., interfacial (IF), partial interfacial (PIF), and pullout failure (PF) modes [37]. As schematically illustrated in Fig. 11, in IF mode, the fracture propagates through the FZ (path A), separating the two sheets apart. In PIF mode, the fracture first propagates along the interface and then redirects perpendicular to the centerline towards the thickness direction (path B). PF mode involves the withdrawal of one sheet from the nugget, and the fracture may initiate in the BM (path C), HAZ (path D), or HAZ/FZ (path E) [80]. IF is accompanied by little plastic deformation and is therefore undesirable as it means low-energy absorption capability. On the other hand, PF is the most desirable mode because it involves more plastic deformation and higher energy absorption and peak load [37, 63, 71, 79, 81].

Generally, nugget size is considered as the main criterion that determines the mechanical performance of spot welds [14, 21, 30, 63, 71, 82]. It has also been shown that for a stack of sheets of same base material, the thinnest sheet thickness, known as governing metal thickness (GMT), generally has the lowest tearing resistance and thus dictates the joint strength [15, 16, 83]. Radakovic and Tumuluru [84] derived the following equations to predict pullout and interfacial failure loads, F_{PO} and F_{IF}, respectively [84]:

$$F_{PO} = k_{PO} \cdot \sigma_{UT} \cdot d.t \quad (2)$$

$$F_{IF} = k_{IF} \cdot \sigma_{UT} \cdot d^2 \quad (3)$$

where k_{PO} (~2.2) and k_{IF} (~0.6) are constants, σ_{UT} is the ultimate tensile shear strength of the base material, d is nugget diameter, and t is the sheet thickness.

Based on Eqs. (2) and (3), pullout failure load strongly depends on the nugget diameter and sheet thickness, while interfacial failure load depends primarily on the nugget diameter.

During TS tests of Al and Mg spot welds, IF is the most commonly observed failure mode [19, 27, 85, 86] because the FZ hardness is comparable to or less than that of the BM [87].

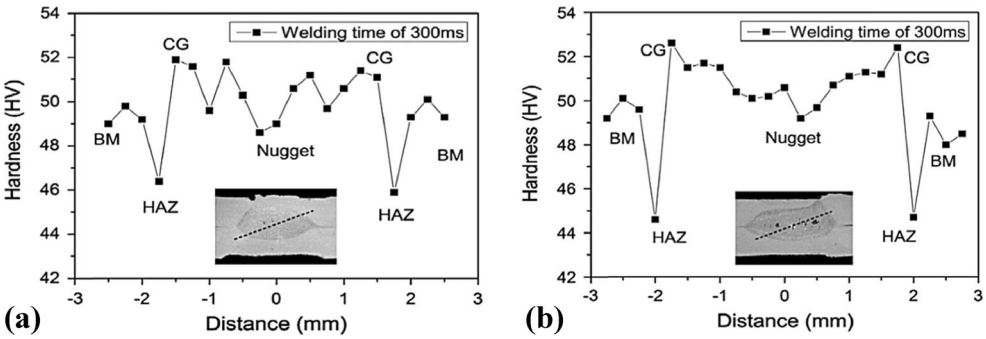

Fig. 10 Typical hardness profile of AA5052 spot weld **a** without EMS and **b** with EMS [30]

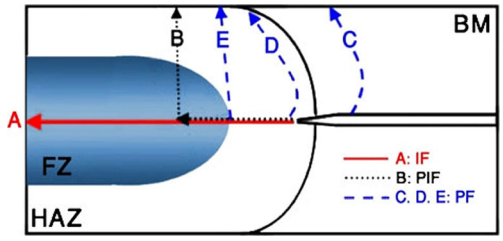

Fig. 11 Schematic representation of main fracture paths during tensile-shear test [80]

For example, Florea et al. [27] have conducted TS tests on samples of 2-mm-thick 6061-T6 Al alloy spot welds, with nugget diameters of 4.5, 5.7, and 6.5 mm. All the samples failed in IF mode, with an average failure load of about 3.1, 4.8, and 6.2 kN, respectively. Observation of the fracture surface revealed a distinctive granular appearance over the entire weld area, with no visible partial thickness fracture. Similarly, Wu et al.[19] welded 2-mm AA6111-T4 Al alloy under different welding conditions to produce two distinct target button diameters of less than 4 $t^{1/2}$ (5.7 mm) and equal to 5 $t^{1/2}$ (7.9 mm), all of which failed in IF mode during TS test, with an average failure load of 3.3 and 4.9 kN [19]. IF, PIF, and PF modes were observed during TS of 1-mm 6082-T6 Al alloy spot welds, depending on the nugget diameter. IF mode occurred for nugget diameters up to 5.1 mm while PF mode occurred for nugget diameters above 5.6 mm. For nugget sizes between 5.1 and 5.6 mm, both failure modes occurred [63]. Furthermore, the authors derived the following equation to predict the critical nugget diameter (d_{cr}) required to ensure pullout failure mode during TS test of heat-treatable Al alloys spot welds [63]:

$$d_{cr} = 4t\frac{HV_{BM}}{HV_N} \quad (4)$$

where t is the sheet thickness; HV_{BM} and HV_N is the hardness of the BM and nugget, respectively.

The TS strength of spot welds of 5xxx series Al alloys has also been studied, in both similar and dissimilar combinations with other alloys [22, 71, 85, 86, 88]. For example, Sun et al. [86] evaluated the mechanical performance of 2-mm-thick similar 5182-O/5182-O alloys and dissimilar 5182-O/6111-T4 Al alloys resistance spot welds and obtained an average peak load of 7.16 and 7.17 kN respectively, with all the samples failing in IF mode [86]. However, Kang et al. [88] reported nugget pullout failure mode, with a maximum tensile shear load of 6.1 kN, when conducting TS test on dissimilar resistance spot weld between 2-mm AA5754 Al alloy and 3-mm Aural2 die casting alloy. The fracture initiated at the notch root and propagated around the nugget on the Aural2 side of the weld [88]. Studies on the TS performance of three-sheet Al resistance spot welds have shown that the peak load increases with increased button diameter and that the failure mode changes from IF to PIF to PF at certain critical nugget diameters [71]. As shown in Fig. 12a, for 2/2/2 mm AA5052 Al alloy spot welds, for the upper interface, the critical button diameter for change in failure mode from IF to PIF (MF) was 5.75 mm and from MF to PF was 6.60 mm. For the lower interface, the critical button diameter for transition in failure mode from IF to MF was 5.35 mm and from MF to PF was 6.40 mm, which are smaller than those of the upper interface, due to Peltier effect [71]. For the 1.0/1.5 interface of 1.0/1.5/2.0 mm configuration, as shown in Fig. 12b, the critical button diameter for transition from IF to MF was found to be 4.45 mm and from MF to PF was 4.90 mm. For the 1.5/2.0 interface, the critical button size transition from IF to MF was found to be 5.00 mm and 7.00 mm from MF to PF. Therefore, to ensure PF, the button size should be larger than 4.90 mm for 1.0/1.5 interface and 7.00 mm for 1.5/2.0 interface [71]

Studies have also shown that the cross-tension strength depends on nugget diameter and sheet thickness and can be affected by defects, such as porosity, around the weld nugget [83, 86]. For instance, the cross-tension failure load of 1.2-mm A 5182-O Al alloy spot welds was found to be 1.69, 2.3, and

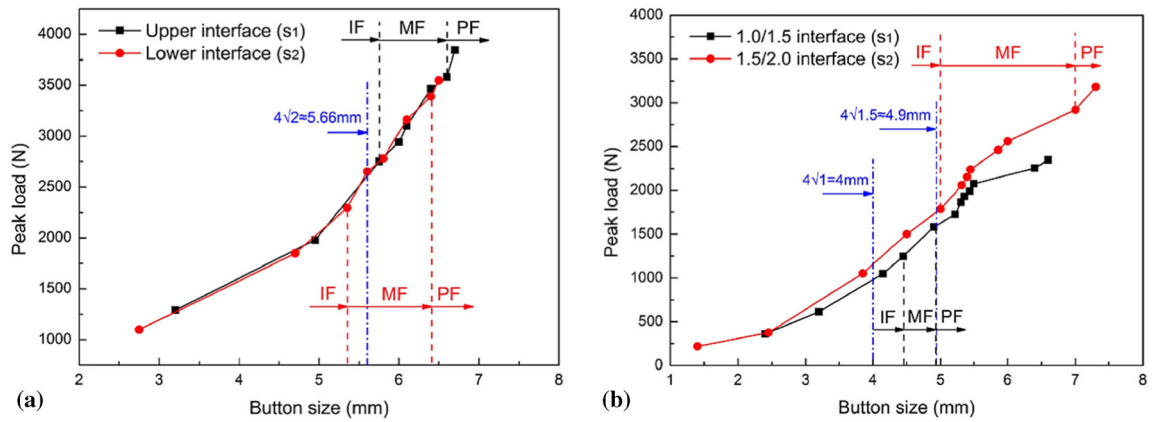

Fig. 12 Effect of button size on the peak load of three-sheet AA5052 Al alloy: **a** 2/2/2 mm configuration and **b** 1/1.5/2 mm configuration [71]

2.68 kN, for welds with nugget diameter of 4.63, 6.35, and 7.93 mm, respectively [85]. Furthermore, Sun et al. [86] conducted cross-tension test on spot welds of 2–mm thick similar 5182-O/5182-O and dissimilar 5182-O/ 6111-T4 Al alloys and obtained an average peak load of 6.05 and 5.95 kN, respectively, with samples failing predominantly in pullout failure mode. It was found that the level of porosity in the nugget influences the cross-tension failure load and that a critical nugget diameter ($D_{critical}$) exists at which pullout failure mode occurs. An analytical failure model was proposed to determine this diameter as follows:

$$D_{\text{critical}} > \frac{3.2t}{f} \tag{5}$$

where t is the sheet thickness; f is the porosity factor, given by:

$$f = \frac{A_{\text{total}} - A_{\text{porosity}}}{A_{\text{total}}} \tag{6}$$

A_{total} is the total area of the fusion zone; $A_{porosity}$ is the area of porosity in the fusion zone.

However, this model is only valid for situations where the weld metal and HAZ hardness/strength are similar to that of the BM. Therefore, it is invalid for spot welds of precipitation-hardening alloys, especially in the T6 condition [86]

6.3 Fatigue

The natural notch that exists at the junction between sheets in spot welds acts as a pre-existing crack or stress concentration site, making them susceptible to fatigue failure. Thus, fatigue is the most critical failure mode for spot-welded and weld-bonded joints. It is therefore of paramount importance to understand the fatigue behavior of spot welds in order to ensure the integrity, durability, and safety of welded structures [18, 65, 87, 89–91]. However, thus far, limited study has been conducted on fatigue behavior of Al spot welds.

Studies have shown that the fatigue behavior of Al spot welds depends on sheet thickness, nugget diameter, loading type, and applied load levels [18, 22, 36]. For example, Shi and Guo [18] studied the fatigue behavior of TS and CP specimens of AA5754 and AA611-T4 Al alloys, at load ratios between 0.1 and 0.3. The load ratio was found to have insignificant effect on the fatigue strength. However, as shown in Fig. 13, a significant improvement of fatigue strength was observed with increase in sheet thickness from 1.0 to 2.5 mm. Furthermore, the fatigue strength of TS specimen was found to be significantly higher than that of CP specimen (Fig. 13), suggesting that the fatigue strength strongly depends on the loading type.

Under cyclic loading conditions, TS specimens of Al alloys spot welds commonly fail in IF mode in low cycle fatigue (LCF) regime (high load levels) [18, 22, 92] and in coupon

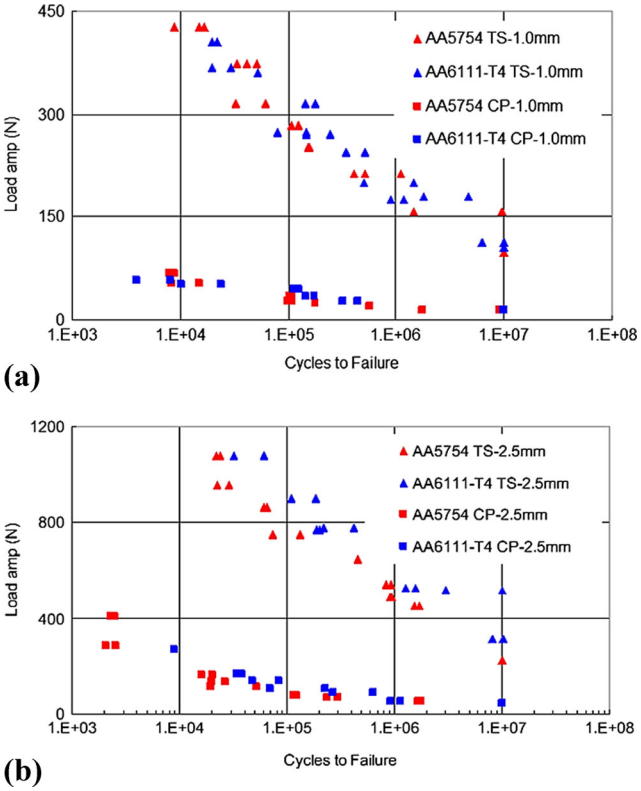

Fig. 13 Comparison of the fatigue behavior of AA5754 and AA6111-T4 Al alloys spot (TS and CP specimens): **a** 1-mm specimens and **b** 2.5-mm specimens [18]

failure mode in high cycle fatigue (HCF) regime (low load levels) [22, 92]. Hassanifard et al. [22] found that the fatigue behavior of 1.2-mm 5083-O Al alloy spot weld improved with increase in electrode force, as shown in Fig. 14. Furthermore, the specimens failed in IF mode at high load levels, e.g., 75 % of load level. On the other hand, button PF occurred at low and intermediate load levels, e.g., 20–50 % of load levels. In both failure modes, cracks initiated from the discontinuity areas near the notch roots and propagated in the HAZ. The secondary crack would always initiate from the opposite side of nugget in which the primary crack initiates [22]. Florea

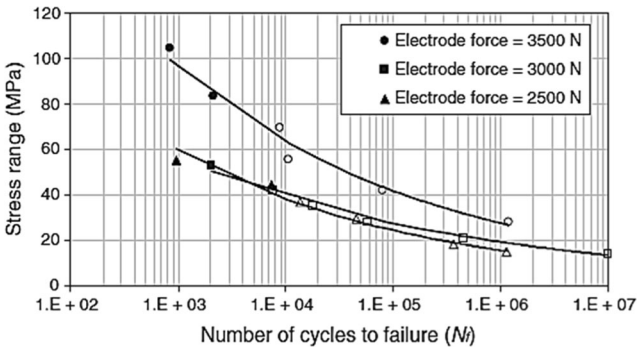

Fig. 14 Fatigue behavior of 5083-O Al alloy spot welds at various electrode force (*open symbols* represent button PF while filled symbols represent IF) [22]

et al. [36] have conducted fatigue tests, at a maximum load of 2.0 kN, on TS specimens of 6061-T6 Al alloy resistance spot welds, having nugget diameters of 4.5, 5.7, and 6.5 mm. The specimen with 4.5-mm nugget diameter was found to have the shortest fatigue life of about 6000 cycles, with samples failing in IF mode, while the specimen with 6.5-mm diameter exhibited the longest fatigue life of approximately 120,000 cycles, with pullout failure mode [36]. However, Gean et al. [85] found, while studying the fatigue behavior of 1.2-mm 5182-0 aluminum Al alloy spot welds, that the nugget diameter has a small effect on fatigue strength under high load levels and no effect under low load/high-endurance (10^6 cycles) conditions [85]

Generally, Al spot welds have lower fatigue strength than equivalent welds in steel [85, 88, 92]. Figure 15 compares the fatigue strengths (in terms of load range) of resistance spot welds of steel, Mg, and Al alloys, in the TS configuration. As shown in the figure, for the same $d/t^{\frac{1}{2}}$ ratio, the fatigue strengths of Al spot welds were found to be comparable to that of Mg alloy but significantly less than that of steel. In the LCF regime, the large difference in fatigue behavior is mainly due to difference in failure mode. While spot welds of Mg and Al alloys fail in IF mode through the FZ, those of steel fail through the HAZ because the HAZ in steel spot welds has lower hardness than the FZ. However, in the HCF, steel, Mg, and Al alloys, spot welds commonly exhibit same type of failure mode (coupon failure through the HAZ). Therefore, in HCF regime, the reason for the superior fatigue behavior of steel spot welds is because of the higher HAZ strength compared to that of Al and Mg alloys [92]. Enhancing electrode force reportedly improves the fatigue strength of Al spot welds by increasing the gap distance between sheets, reducing the sharpness and the stress concentration at the notch and thus delaying crack initiation and growth [22, 85, 93]. For example, for 1.2-mm 5182-0 Al alloy spot welds, the fatigue load at 10^6 cycles was found to be 15 % higher when electrode force was increased from 4 to 6.5 kN and 15 % lower when it was decreased from 4 to 1.5 kN [85].

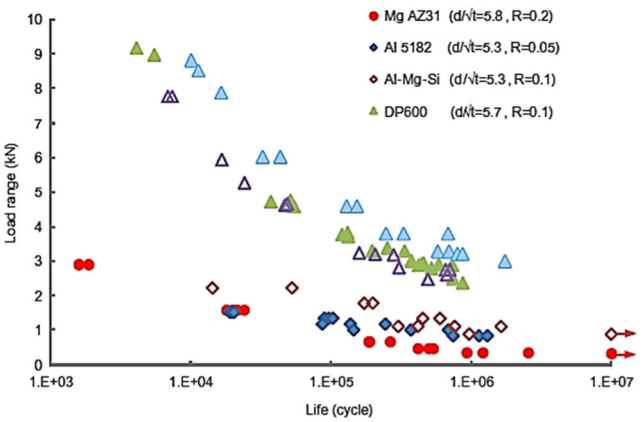

Fig. 15 Comparison between the fatigue behavior of Mg alloy, Al alloys, and steel spot welds in TS configuration ($d/\sqrt{t}$ values are in $\sqrt{mm}$) [92]

7 Resistance plug welding

7075 Al alloy is widely used in the automotive structures in such applications as body panels, brake housings, brake pistons, air deflector parts, and seat slides [21, 78, 94]. It is, however, difficult to obtain high-quality welds in this alloy due to its susceptibility to hot cracking, which is caused by the presence of relatively high amount of Cu and the wide range of melting point, with a low solidus temperature [21, 95]. To produce reliable welds in this alloy, Feng et al. [21] proposed a novel technique known as resistance plug welding (RPW). In this technique, circular holes were produced at the center of the overlap area of the 7075 Al alloy sheets and a filler rod made of 5052 Al alloy, which has better weldability than 7075 Al alloy, was inserted into the holes, followed by RSW. The joints produced by this technique were of better quality than those produced by conventional RSW. Defects, such as porosity and hot cracking, which were observed in the joints produced by conventional RSW, were not produced by RPW because of the superior weldability of the inserted 5052 Al alloy. Furthermore, the RPW produced joints with larger nugget diameters and higher peak loads and energy absorption. For the RSW joints, the maximum nugget diameter, peak load, and energy absorption was found to be 4.7 mm, 1.23 kN, and 0.65 J, respectively. The RPW was found to increase the maximum peak load by 20.2 % and the maximum energy absorption by 177 % [21]. Although this technique seems promising, further study is required to see how it can be improved. For example, the dimensions of the filler rod can be optimized and other insert alloys can be tried.

8 Residual stresses in Al spot welds

Residual stresses are formed in spot welds due to non-uniform temperature distribution during the welding process, as well as due to the phase changes that occur during solidification of the weld metal. They promote crack propagation and impair fatigue behavior [22, 96–99].

Studies on the development of residual stresses in Al alloy resistance spot welds have shown that the residual stresses in the nugget area are predominantly tensile. The highest tensile residual stress occurs around the center of the nugget and then decreases slightly towards the edge of the nugget [93, 96, 98, 100]. For example, the maximum residual stress in resistance spot weld of 5754 Al alloy was found to be 75 MPa (close to the yield strength of the BM), at the center of the nugget. Away from the center of the nugget, at a distance equal to half the thickness of the nugget, the value decreased to 50 MPa

[98]. Neutron scatter diffraction technique was used to quantify the three dimensional residual stress fields in 2-mm-thick 6061-T6 Al alloy resistance spot welds, i.e., in-plane longitudinal (σ_{11}), in-plane transversal (σ_{22}), and normal (σ_{33}) residual stresses. Measurements were taken in the center section of the joint (middle), 1 mm above the mid-plane (top), and 1 mm below the mid-plane. As shown in Figs. 16 and 17, the residual stresses were found to be in the range of 30–120 MPa (the highest value being approximately 40 % lower than yield strength of the BM). For σ_{11} component, the stresses are positive (tensile) in the horizontal direction but vary from ±100 MPa in the vertical direction (Fig. 16). On the other hand, the σ_{22} component is mostly positive in both directions (Fig. 17). The values of σ_{33} were found to be negligible and can thus be ignored in weld joint design [41]. It is important to state that increasing the electrode force was found to be beneficial in reducing the amount of tensile residual stresses [22, 93]

9 Effect of welding parameters

The quality and performance of resistance spot welds are influenced by heat input, which in turn depends on welding parameters, primarily welding current, welding time, and electrode force [37, 45, 101–104]. It is important to select the correct welding parameters to produce a reliable and sound joint with the desired geometric features and mechanical properties [51]

9.1 Effect of welding current and time

Welding current is the most influential parameter in RSW. Generally, a low-current results in low heat input, an undersized size, and poor penetration. Increasing the current leads to an increase in heat generation, nugget size, and tensile shear load [14, 26, 30, 36, 63]. Because of their high thermal conductivity, high welding current and short welding time are required for RSW of Al alloys. However, excessive welding current could lead to excessive heat generation, severe expulsion, poor joint quality, and appearance [26, 27, 44, 62, 63].

Figure 18 shows the effect of welding current on the strength of 2-mm 6061-T6 Al alloy spot weld at various welding times and a constant electrode pressure of 5 kg/cm^2 [67]. Over the range of current studied, at a given welding time, the tensile shear load increased with increase in welding current due to increase in nugget size [67]. Maximum tensile shear load of about 2.75 kN was obtained at a welding current of 20 kA and 8 cycles welding time [67]. In another study, also conducted on 2-mm 6061-T6 at 4.03 kN electrode force and 4-cycle welding time, it was found that increasing the welding current from 36 to 40 kA resulted in an increase in nugget diameter from 5.8 to 8.5 mm, with corresponding increase in strength from 3.3 to 4.9 kN [73]. Similarly, for 1-mm 6082-T6 Al alloy, at 2-cycle welding time and 3.24 kN electrode force and in current range of 23–29 kA, the nugget diameter was found to increase from 4.2 to 6.5 mm, with corresponding increase in joint strength from 2.1 to 3.3 kN [63].

Although the nugget diameter and joint strength increase with increase in welding current, the electrode imprint/indentation also increases, even at constant electrode force [27, 63]. A spike in electrical current could create a large imprint and potential burn-through effect, especially on thins sheets, affecting joint quality and appearance [27]. In one study, carried out on 1-mm 6061-T6 Al alloy, at an electrode force of 3.3 kN and 2-cycle welding time, a sudden increase in indentation was observed at a welding current of 27 kA, and about 15 % reduction in the initial thickness of the sheets was obtained at a welding current of 28 kA [63]. Figure 19 depicts the 3D laser profilometer images of electrode imprints on the surface of 2-mm 6061-T6 Al alloy as a function of welding current. As shown, the indentation depth on the top welded sheet was found to increase linearly with increase in welding current, with a mean average value of 32, 40, and 53 μm at welding current of 26, 30, and 38 kA, respectively. However, the indentation depth on the bottom welded sheet exhibits a random tendency due to spatter from the weld process, with mean average value of 14, 34, and 32 μm, at of 26, 30, and 38 kA, respectively [27]. Thus, although it is favorable to

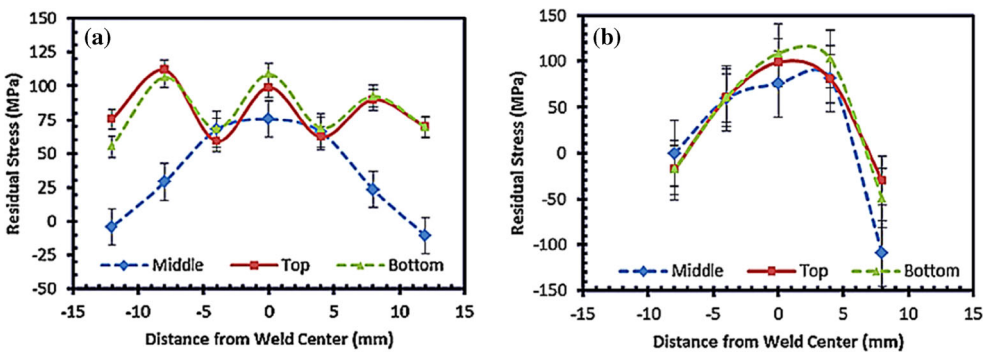

Fig. 16 σ_{11} stresses in **a** horizontal direction and **b** vertical direction [41]

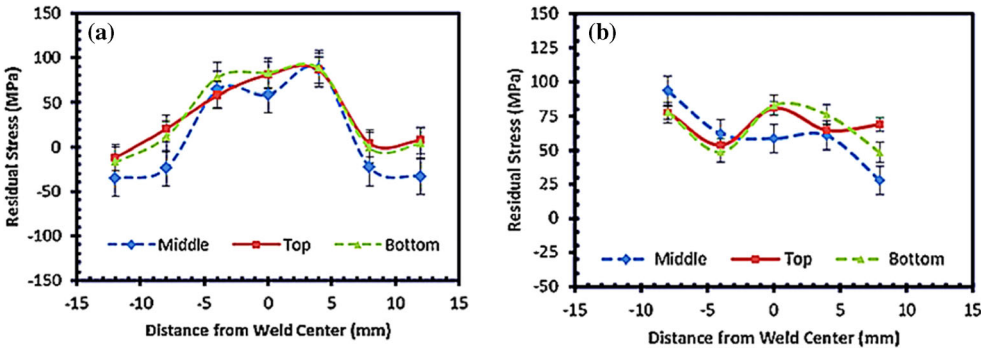

Fig. 17 σ_{22} stresses in **a** horizontal direction and **b** vertical direction [41]

select high welding currents for Al alloys, the values should not be unnecessarily high.

The effect of welding time on heat input is similar but less significant. This is because the heat input is proportional to the square of the current and to the first power of time on Joule's law (Eq. 1). As the welding time increases, the heat input and in turn the nugget size also increase [14, 30, 73, 105]. However, too long a welding time coarsens the microstructure of the weld nugget and heat-affected zone and thus affects the hardness [63]. It also results in increased electrode heating and wear [44]. Figure 20 depicts the effect on welding time on the strength of 2-mm 6061-T6 Al alloy spot welds, produced at constant electrode pressure of 5 kg/cm^2 and various welding currents. As shown in the figure, at a particular welding current, increase in welding time up to 8 cycles increases the tensile shear load. However, further increase in welding time leads to reduction of joint strength, which was attributed to expulsion. A maximum tensile shear load of 2.75 kN was obtained at a welding current of 20 kA and 8-cycle welding time [67]. Similarly, in another study conducted on 2-mm 6061-T6 Al alloy at 4.36 kN electrode force and welding current of 36 kA, it was found that by increasing the welding time from 4 to 8 cycles, the nugget diameter and failure load increased from 5.8 to 8 mm and 3.3 to 4.3 kN, respectively. Further increase in welding time also resulted in expulsion [73]. Furthermore, evaluation of the effect of welding time on the properties of 1-mm 6082-T6 aluminum alloy, conducted at constant welding current of 26.4 kA and electrode force of 3.24 kN, has shown that the nugget diameter and failure load increased from approximately 1.5 mm and 0.7 kN, respectively, at 1 cycle to 5.6 mm and 2.8 kN at 3 cycles and remain approximately constant for current times beyond 3 cycles [63]. Thus, for any particular sheet thickness and welding current, it is unnecessary to prolong the welding time beyond a critical value.

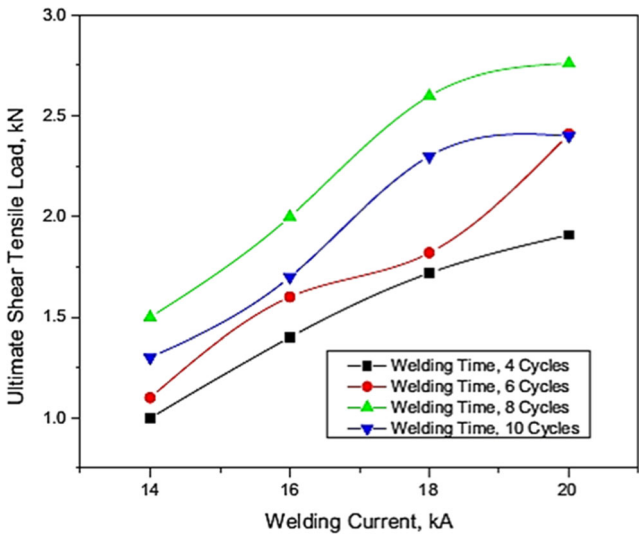

Fig. 18 Influence of welding current on tensile shear strength of 6061-T6 Al alloy spot welds [67]

9.2 Electrode force

Electrode force influences the joint properties mainly through its effects on contact resistance and contact area. Insufficient electrode force would result in high contact resistance, excessive heat generation, expulsion, and poor joint quality [30, 37, 106, 107]. High electrode is required in RSW of Al alloys to squeeze and break down the oxide layer and thus reduce the contact resistance [25, 44, 54, 55, 63]. However, very high electrode force could lead to severe indentation, sheet separation, and distortion [47, 58, 63, 106]. Furthermore, the nugget diameter and joint strength tend to decrease with the increase of electrode force above a critical value, due to increase in contact area, reduction in current density, and increased heat dissipation [26, 30, 63, 105]. Afshari et al. [73] studied the effect of electrode force on the nugget diameter and tensile shear load of 2 mm 6061-T6 Al alloy spot weld, at a welding current of 36 kA and welding time of 4 cycles. As shown in Fig. 21, increasing the electrode force from 3.67 to 4.58 kN led to an increase of the nugget diameter from 5.5 to 8.1 mm and that of failure load from 3.1 to 4.41 kN. However, when the electrode force was further increased to 4.77 kN, the nugget size and failure load decreased to 7.7 mm and 4 kN, respectively [73]. As shown in Fig. 22, for 1-mm 6082-T6 Al alloy, at a welding current of 26.4 kA and welding time of 2 cycles, increasing the electrode force beyond approximately 4 kN leads to a drop in nugget [63]. A similar observation was

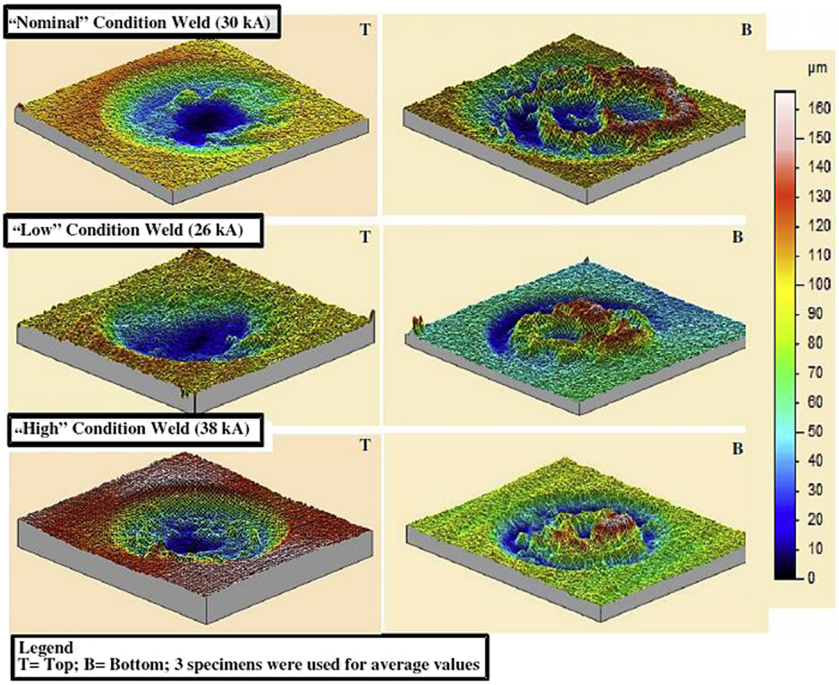

Fig. 19 Axonometric 3D weld profiles for top (*T*) and bottom (*B*) welds at different welding currents. The *dark blue* indicates depth, while the *red* and *pink* indicate height. The scanned surface was 20 mm × 20 mm [27]

made for 2-mm AA5052 Al alloy spot welds. The nugget diameter and strength increased with increased electrode force up to 4 kN and dropped thereafter [30].

10 RSW of Al alloys to other alloys

To improve performance and cost-effectiveness, and to exploit the advantages of different materials, hybrid structures, such as Al/steel, Al/Mg, Al/Ti, and Mg/steel, are widely used in many applications. It is thus important to understand the joining mechanism and performance of dissimilar joints

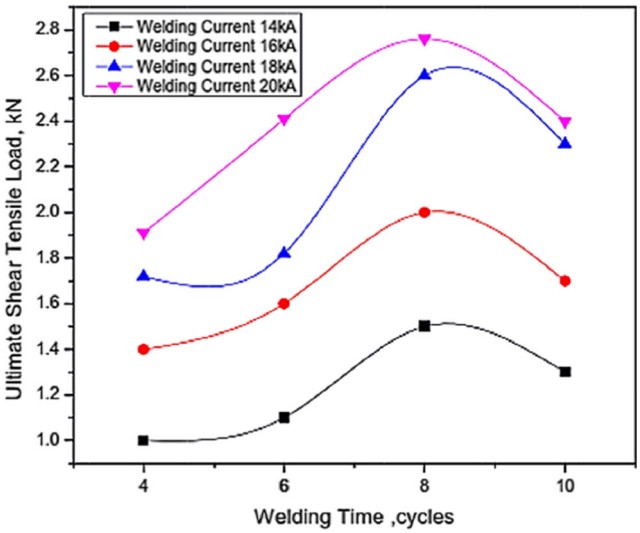

Fig. 20 Effect of welding time on tensile shear strength of 2 mm 6061-T6 Al alloy resistance spot welds [67]

10.1 RSW of Al alloys to steels

Steel is currently the primary structural material in the automotive industry. Therefore, joining Al to steel is indispensable. However, because of the large difference in physical and thermal properties between Al alloy and steel (Table 1), welding them together is difficult. The nearly no intersolubility between them results in the formation of brittle Al-rich intermetallic compounds (IMCs) at the interface, mainly Fe_2Al_5 and $FeAl_3$ [61, 62, 66, 109–114]. A study of the kinetics of growth of the IMC layer has shown that its formation and growth are mainly driven by reactive diffusion between Fe and Al atoms and that its thickness and morphology depend on interaction time between liquid Al alloy and solid steel and also on the interfacial temperature [61]. Generally, the morphology and thickness of the IMC layer varies along the Al/steel interface, with maximum thickness being obtained at the center, due to its higher interfacial temperature and longer reactive diffusion time [61, 62, 64, 66, 109–113].

Zhang et al. [62] joined 1-mm H220YD galvanized high-strength steel to 1.5-mm 6008 Al alloy directly by RSW. The joint was found to be a special brazed joint where the melted Al alloy spread on solid steel surface, forming an Al alloy nugget and a steel HAZ. A similar observation was made during the dissimilar RSW of 5052 Al alloy/St-12 (DC 01) steel and 5052 Al alloy/low carbon galvanized steel [114]. IMC layer consisting of Fe_2Al_5 phase, with lath-like or tongue-like morphology was observed beside the steel, and Fe_4Al_{13} phase, with needle-like morphology beside the Al alloy nugget. The thickest IMC comprised of ~5-μm-thick

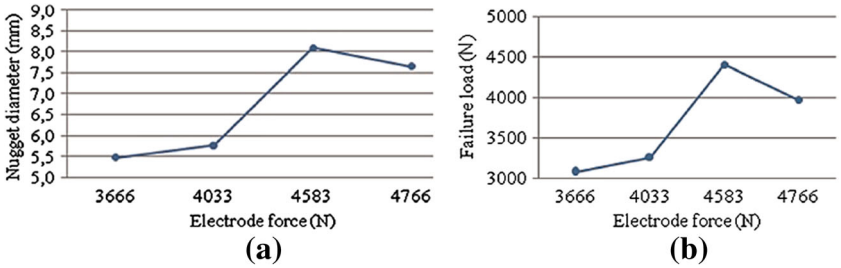

Fig. 21 Effect of electrode force on **a** nugget diameter and **b** failure load (welding current 36 kA; welding time 4 cycles) [73]

Fe_2Al_5 and at least 2.5-μm-thick Fe_4Al_{13}. As shown in Fig. 23, the IMC layer exhibited the highest hardness compared to the Al and steel sides, with average nanohardness value of approximately 8.7 and 6.5 GPa for Fe_2Al_5 and Fe_4A1_3 layers, respectively. The average hardness of the Al alloy nugget and galvanized steel near the interface was found to be approximately 1.1 and 2.1 GPa, respectively. During TS test, IF mode occurred. The cracks initiated in the Fe_2Al_5 layer and propagated mainly through the IMC layer and partially through the FZ. A maximum tensile shear load 3.31 kN was obtained [62]. To improve the weldability and joint strength, another study was conducted using optimized electrode morphology, involving a planar circular tip electrode (with tip diameter of 10 mm) on the steel side and a spherical tip electrode (with spherical diameter of 70 mm) on the Al side. This resulted in wider and more homogeneous current density distribution and reduced interfacial temperature. An IMC layer, composing of Fe_2Al_5 and Fe_4Al_{13}, with maximum thickness of about 4.0 μm was formed at the interface, and a tensile shear load of 5.4 kN was obtained [66].

10.1.1 RSW of Al/steel with cover plates

In order to produce reliable joints under relatively low welding current condition, Qiu et al. [109–113] applied the technique

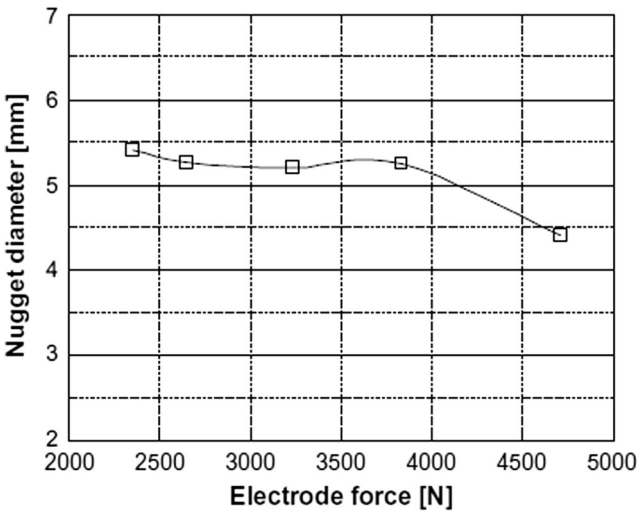

Fig. 22 Effect of electrode force on nugget diameter of 1-mm 6061-T6 Al alloy spot weld at 26.4 kA and 2 cycles [63]

of RSW with cover plate to join 1-mm A5052 Al alloy/1-mm SPCC steel and 1-mm A5052 Al alloy/1-mm SUS304 stainless steel dissimilar joints. In both cases, the cover plate was placed on the Al sheet. The details of this technique can be found in the pioneer work of Qiu et al. [48]

Figure 24a, b show a typical SEM image of the interface of A5052/ SPCC steel and A5052 Al alloy /SUS304 dissimilar joints, respectively [111]. As shown in the figure, for A5052 Al alloy /SPCC steel, the reaction layer exhibited a tongue-like morphology adjacent to the steel side and a fine needle-like morphology on the Al side. On the other hand, for the A5052 Al alloy/SUS304 steel, the reaction layer had a flat front on the steel side and a serrate morphology on the Al side. Characterization of the interfaces by TEM reveals that the reaction product in A5052 Al alloy/SPCC steel joint is composed of Fe_2Al_5 adjacent to the steel and $FeAl_3$ adjacent to the Al side [113]. For A5052 Al alloy/SUS304 steel joint, it is composed of a mixed layer of Fe_2Al_5 and $FeAl_3$ beside the Al alloy and an approximately 35-nm-thick layer of $FeAl_2$ on the steel side. Moreover, a reaction block of hexagonal AlFeCr ($a = 2.451$ nm and $c = 0.758$ nm) was observed in Al alloy near the joint interface [110]. At all welding currents, the reaction layer was found to be thinner at the A5052 Al alloy/SUS304 steel interface than at the A5052 Al alloy/SPCC steel because the presence of Cr in SUS 304 steel reduces the activity coefficient of Al atoms, leading to low growth rate of Fe_2Al_5. During TS test, fracture occurred in the reaction layer in the A5052 Al alloy/SPCC steel joint and in the A5052 Al alloy in A5052 Al alloy/SUS304 steel joint [112]. A maximum tensile shear load of 6.5 and 4.68 kN was obtained for the A5052 Al alloy/SUS304 steel and A5052 Al alloy/SPCC steel joints, respectively [112]

10.1.2 RSW of Al alloy/steel with transition materials

In attempts to restrain the formation of the brittle IMCs and improve the weldability of Al/steel resistance spot welds, different transition materials/interlayers, such as Al clad steel strips [115–117], pure Al alloy [118], Al-Si alloy [64], Al-Mg alloy [119], Al-Cu alloy [105], and Cu coating [26], have been used. For example, Oikawa et al. [116] applied RSW to join 0.8-mm-thick cold rolled steel (EDDQ) and 1-mm Al alloy (Al-5·5 Mg-O) sheets using 0.77-mm Al clad steel sheet

Table 1 Comparison between properties of magnesium, aluminum, and iron [108]

Properties	Magnesium	Aluminum	Iron
Ionization energy (eV)	7.6	6	7.8
Specific heat (J kg^{-1} k^{-1})	1360	1080	795
Specific heat of fusion(J/kg)	3.7×10^5	4×10^5	2.7×10^5
Melting point (°C)	650	660	1536
Boiling point (°C)	1090	2520	2860
Viscosity (kg m^{-1} s^{-1})	0.00125	0.0013	0.0055
Surface tension (Nm^{-1})	0.559	0.914	1.872
Thermal conductivity (Wm^{-1} k^{-1})	78	94.03	38
Thermal diffusivity (m^2 s^{-1})	3.73×10^{-5}	3.65×10^{-5}	6.80×10^{-6}
Coefficient of thermal expansion (1/k)	25×10^{-6}	24×10^{-6}	10×10^{-6}
Density (kg/m^3)	1590	2385	7015
Elastic modulus (N/m^3)	4.47×10^{10}	7.06×10^{10}	21×10^{10}
Elastic resistivity (μΩm)	0.274	0.2425	1.386
Vapor pressure (Pa)	360	10^{-6}	2.3

as insert metal (produced by hot rolling 0.4-mm cold rolled steel sheet and 0.6-mm pure Al sheet). The strength of the joint was found to be higher than that of direct joint and of the same order as that of Al/Al similar joint. The maximum value of tensile shear and U-tension strengths of the direct joint was about 2.4 kN/spot and 0.6 kN/spot, respectively, while that of the joint with insert was found to be about 3.6 kN/spot and 1.5 kN/spot, respectively [116]. However, although the utilization of Al clad steel strip is beneficial in improving the strength of Al/Steel dissimilar joints, cost and difficulty in fabricating the strip would restrict its application.

Recently, Zhang et al. [64] investigated the resistance spot weldability of dissimilar joint between 1-mm H220YD high strength steel and 1.5-mm 6008-T6 Al alloy with 4047 AlSi12 interlayer of different thicknesses (100, 200, 300, and 400 μm). The 4047 $AlSi_{12}$ interlayer was found to restrict the formation and growth of brittle IMCs. Instead, IMC composed of $Fe_2(Al, Si)_5$ and $Fe_4(Al,Si)_{13}$ was formed at the steel/Al interface. With increasing interlayer thickness from 100 to 400 μm, the thickness of the IMC layer decreased from 1.8 to 0.6 μm (the thickness of IMC layer in the interlayer-free joint was about 4.0 μm). Furthermore, the morphology of the IMC layer changed from dual-layered (with tongue-like structure beside steel and needle-like structure adjacent to aluminum nugget) with interlayer thickness of 100–200 μm to single-layered serrated-shaped structure with interlayer thickness of 300–400 μm. And, as shown in Fig. 25, the tensile shear load of the joint increased with interlayer thickness, reached a maximum of 6.2 kN with interlayer thickness of 300 μm (which is significantly higher than that of the interlayer-free joint, 5.4 kN) [64]. More recently, 80-μm-thick Al-Mg alloy (80 wt% Al and 20 wt% Mg) was used to join 2-mm A6061-T6 alloy and 2-mm 304 stainless steel, producing a maximum tensile shear load of 8.4 kN (the TS strength of the interlayer-free joint was about 4.8 kN). Two-micrometer-thick IMC layer composing of Fe_2Al_5 was observed at the interface. The fatigue behavior of the joint in TS configuration was also evaluated. The fatigue limit of the joint, which was defined as the runout load at 10^7 cycles, was found to be 1.75 kN. The fatigue fracture mode was dependent upon the load levels. Plug fracture occurred at high load levels (Pmax ≥3 kN), IF mode at medium load levels (2.25 kN ≤ Pmax ≤ 3 kN), and through thickness fracture at low load levels (Pmax ≤ 2.25 kN) [119].

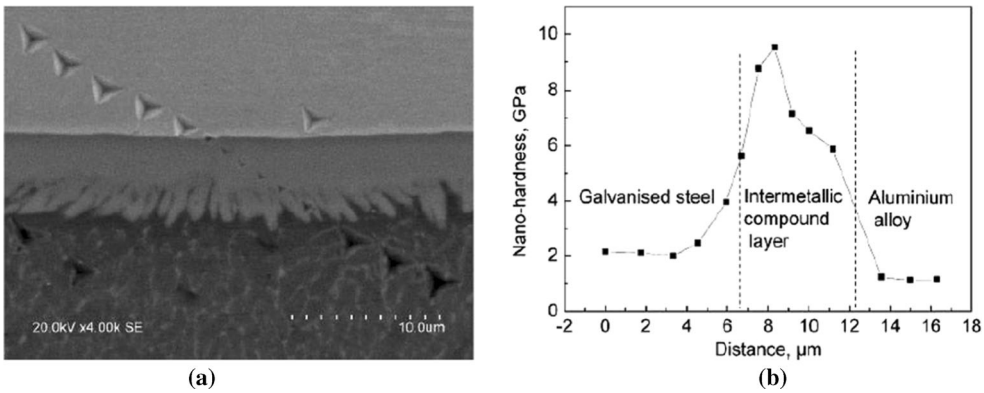

Fig. 23 Nanohardness tests across galvanized steel/Al alloy resistance spot weld: a nanoindents; b nanohardness profile [62]

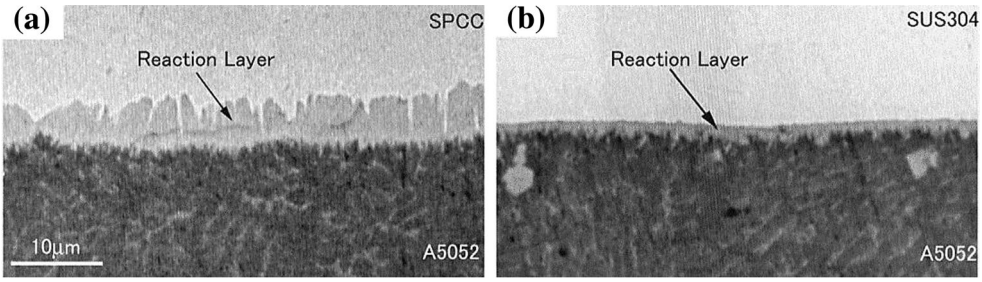

Fig. 24 SEM images of the interface of **a** A5052 Al alloy/ SPCC steel and **b** A5052 Al alloy /SUS304 stainless steel dissimilar joints [111]

A significant improvement in tensile shear load of 1-mm A6061 Al alloy/1 mm Q235 steel was obtained, from 2.8 kN (for direct joint) [120] to 3.8 kN by employing 0.03-mm AlCu28 foil interlayer [105]. The strength further increased to 4.6-kN when the Q235 was copper-coated (coating thickness of 2 μm), suggesting that copper plating can improve the strength of Al/steel dissimilar joint [26].

10.1.3 RSW of Al/steel with a rivet

Seeking to further improve the strength of dissimilar Al/steel resistance spot welds, the technique of resistance spot welding with a rivet, also called resistance element welding, was recently introduced [120, 121]. In this technique, a technological hole is drilled at the center of the overlap area of the Al alloy, and then a steel rivet is inserted into the hole before welding [120, 121]. The technique was first tried by Qiu et al. [120] to weld A6061 Al alloy/ Q235 steel, each 1-mm thick. The diameter and length of the rivet conformed to diameter of the hole and Al sheet thickness, respectively. The maximum tensile shear load of the joint was found to be 3.85 kN, which is significantly higher than that of the joint produced by conventional RSW (2.8 kN). An approximately 4-μm-thick FeAl reaction layer was observed at the rivet/Al alloy interface and $FeAl_3$ at the steel/Al alloy interface [120].

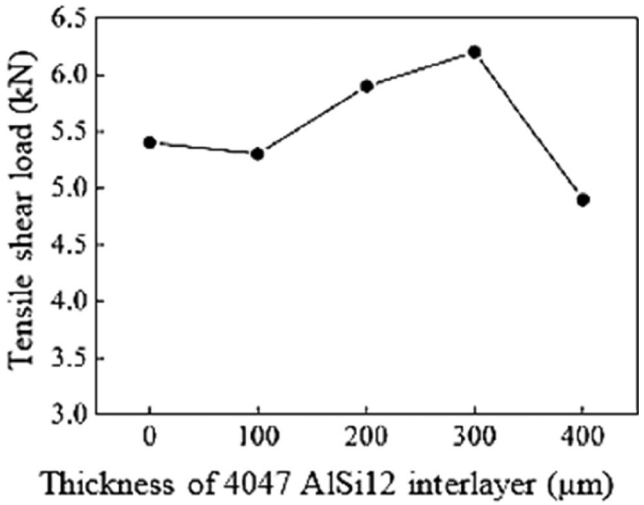

Fig. 25 Effect of 4047 AlSi12 interlayer thickness on tensile shear load of welded joints [64]

More recently, Ling et al. [121] employed the technique to join a 2-mm 6061 Al alloy to 1.8-mm uncoated 22MnMoB boron steel, using Q235 steel rivet with 5-mm diameter. A very strong joint, with a maximum tensile shear load of 7 kN and energy absorption of 11.38 J, was obtained. On the other hand, conventional RSW produced a weak joint, with a maximum tensile shear load of 957 N and a maximum peak energy absorption of 0.09 J. Some joining was also achieved between the Al sheet and the Q235 rivet. Four-micrometer-thick IMC, composing of FeAl, Fe_2Al_5, and $FeAl_3$, was also observed at the rivet/Al interface. Furthermore, compared to the conventional RSW, the technique required the application of relatively lower welding current as it involves welding steel to steel. [121]. The technique can be improved further by optimizing the length and diameter of the rivet [120].

Table 2 compares the strength of Al/steel resistance spot welds, obtained using different techniques. From the strengths obtained, it can be seen that the use of interlayers, resistance element welding, RSW with cover plates, and the use of optimized electrode morphology are promising techniques in suppressing the IMC and improving joint strength. For the interlayer added joint, the highest strength was obtained using Al-Mg alloy interlayer, followed by 4047 $AlSi_{12}$ foil. Other interlayers should be tested to exploit the full potential of this technique. The technique of RSW with a rivet appears to be promising and further study is needed to improve the technique, for example, by optimizing the length and diameter of the rivet. For the interlayer-free joints, the technique of RSW with cover plate gave the highest strength value, followed by optimized electrode design.

10.2 RSW of Al/Mg alloys

Mg is the lightest structural metal, with a density of approximately one fourth that of steel and two thirds that of Al. Thus, joining Al to Mg alloys would lead to significant weight savings. However, it is a very challenging task due to differences in physical and metallurgical properties (Table 1), which promote the formation of brittle IMCs, such as $Mg_{17}Al_{12}$ and Mg_2Al_3 [8, 35, 122–124].

A study of the mechanism of nugget formation during dissimilar RSW of 2024 Al alloy/AZ31B Mg alloy has shown that a certain amount of plastic deformation occurred at the

Table 2 Comparison of the tensile shear strength of Al/Steel dissimilar joints using different techniques

Materials combination	Joining Technique	Transition material	IMCs	IMC layer thickness	TS strength (kN)	Reference
1-mm H220YD galvanized high strength steel/1.5 mm 6008 Al alloy	Conventional RSW	–	Fe_2Al_5 and Fe_4Al_{13}	At least ~7.5 μm	3.31	[62]
	Conventional RSW with optimized electrode morphology	–	Fe_2Al_5 and Fe_4Al_{13}	4.0 μm	5.4	[66]
1-mm A5052 Al alloy/1-mm SPCC steel	Conventional RSW	300-μm 4047 AlSi12	$Fe_2(Al,Si)_5$ and $Fe_4(Al,Si)_{13}$	0.6 μm	6.2	[64]
1-mm A5052 Al alloy/1-mm SUS304	RSW with cover plate	–	Fe_2Al_5, $FeAl_3$ and $FeAl_2$	Maximum thickness of 7 μm	4.68	[112, 113]
		–	Fe_2Al_5 and $FeAl_3$	Maximum thickness, of 2.5 μm	6.5	[110, 112]
2-mm A6061-T6 alloy/2-mm 304 stainless steel	Conventional RSW	–	Not reported	Not reported	4.8	[119]
2-mm A6061-T6 alloy/2-mm 304 stainless steel	Conventional RSW	80-μm thick Al-Mg alloy	Fe_2Al_5	2 μm	8.4	[119]
0.8-mm cold rolled steel (EDDQ)/1-mm Al alloy (Al-5·5 Mg-O)	Conventional RSW	–	Not reported	Not reported	2.4	[116]
	Conventional RSW	0.77-mm aluminum clad steel	Not reported	Not reported	3.6	[116]
1-mm A6061 Al alloy/1-mm Q235 steel	Conventional RSW	–	Not reported	Not reported	2.8	[120]
		0.03-mm AlCu28 foil	Not reported	Not reported	3.8	[105]
	RSW with a rivet	–	FeAl and $FeAl_3$ at rivet/Al interface	4 μm	3.85	[120]
1-mm A6061 Al alloy/1-mm copper-coated Q235 steel	Conventional RSW	–	Not reported	Not reported	4.6	[26]
2-mm 6061 Al alloy/1.8-mm uncoated 22MnMoB boron steel	Conventional RSW	–	Not reported	Not reported	0.957	[121]
	RSW with a rivet	–	FeAl, Fe2Al5, and FeAl3 at rivet/Al interface	4 μm	7	[121]

interface of the joint and that with increased heat input, the Mg alloy was further softened, thus expanding the plastically deformed region. The Al alloy protruded into the Mg alloy, distorting the weld line and forming a wavelike appearance. These protruded regions served as favorable sites for the mixing of Al and Mg and consequently nugget formation. Energy spectrum analysis showed that the nugget consisted mainly of $Al_{12}Mg_{17}$ IMCs, and the hardness value of the nugget was found to be significantly higher than those of Al and Mg base metals, as shown in Fig. 26 [125]. Similarly, Hayat [35] observed Al_3Mg_2 and $Al_{12}Mg_{17}$ IMCs at the nugget zone of AZ31 Mg alloy/1350 Al dissimilar joint, and due to the presence of these IMCs, the average hardness of the nugget (190 ± 10 HV) was found to be significantly higher than that of the Mg (73 ± 5 HV) and Al (40 ± 5 HV) sides. The high hardness of the nugget would induce microcraking at the joint interface. Observation of the fracture surface of the joint revealed brittle morphology, with distinctive characteristics of brittle intermetallics, as shown in Fig. 27 [35].

10.2.1 RSW of Al/Mg alloys with interlayers

As mentioned in the preceding section, direct welding of Al to Mg alloys results in the formation of brittle to IMCs, which impair the mechanical performance the joint. Therefore, it is imperative to develop means of controlling the formation of IMCs [124].

Interlayers can be used as barrier materials to prevent or restrict the mixing of Al and Mg and therefore suppress the formation of brittle IMCs [124, 126, 127]. Ni, with a melting point of 1455 °C, which is remarkably higher than that of Mg (650 °C) and Al (660.42 °C), could prevent the mixing of Al and Mg when used as an interlayer. Furthermore, Al-Ni and Mg-Ni IMCs are less brittle than Al-Mg IMCs [127]. Thus, Penner et al. [127] explored the feasibility of using Ni based

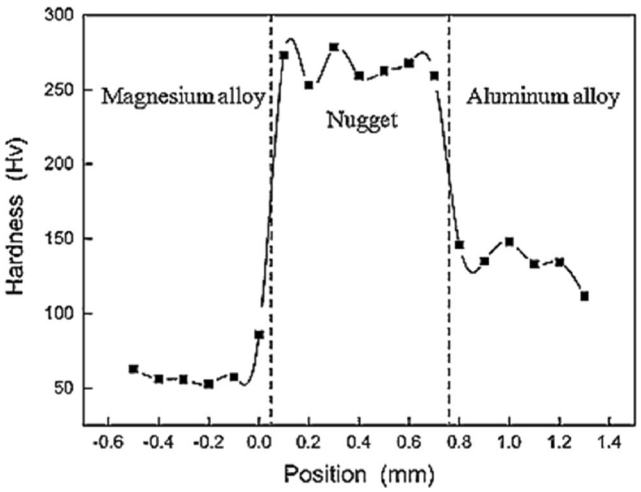

Fig. 26 Microhardness profile of AZ31B Mg alloy/2024 Al alloy resistance spot weld [125]

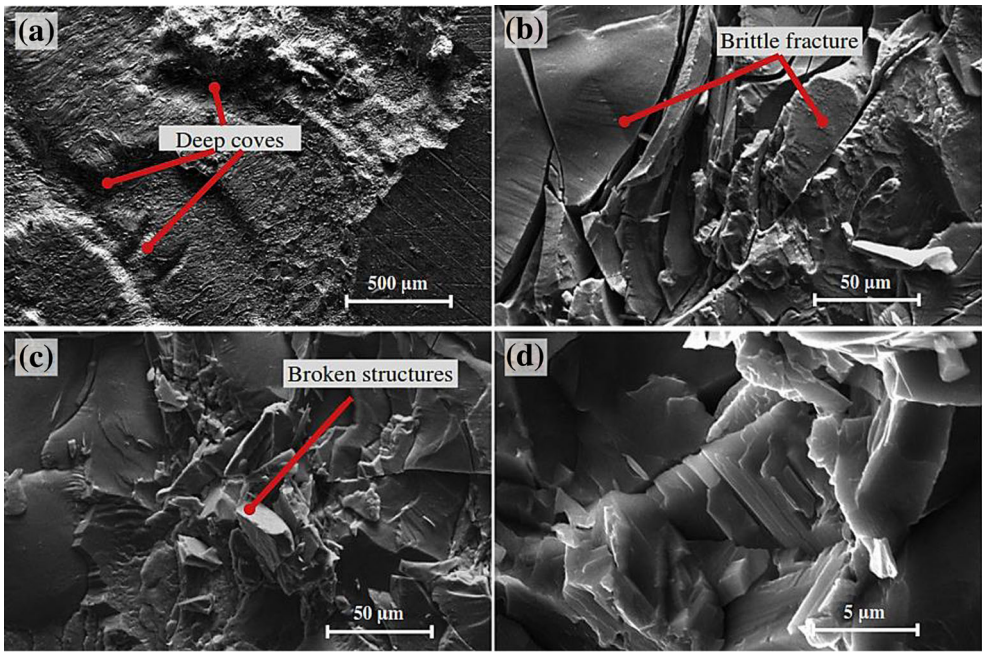

Fig. 27 The fracture surface morphology on the Mg side of direct Al/Mg resistance spot weld: (**a**) macroscopic fracture morphology (100 x); microscopic fracture morphology (**b**) 2,000 x (**c**) 10,000 x and (**d**) 10,000 x

interlayers (0.2-mm pure Ni foil and 0.2-mm gold-coated Ni foil) to join 2-mm-thick AZ31B Mg alloy and 2-mm 5754 Al alloy by RSW. Although the use of pure Ni interlayer could not produce a metallurgical bond between the Mg and Al alloys, the gold-coated Ni interlayer effectively suppressed the formation of Al-Mg IMC and significantly improved the metallurgical bonding between the Mg and Al alloy. The Al alloy was joined to the interlayer by direct weld-brazing in the nugget center and by brazing through Au-based filler metal at nugget edges. On the other hand, the Mg alloy was joined to the Ni mainly through different Au- rich phases, such as Mg_3Au IMC layer and Au-Mg eutectic. Thus, a strong joint with an average peak load of 4.69 kN (90 % of the strength of optimized AZ31B/AZ31B spot welds) was produced [127]. The failed attempt of Penner et al. [127] to join Mg to Al alloys with pure Ni interlayer by RSW was attributed to the application of low heat input [128]. Therefore, in a more recent study, which also employed 0.2-mm-thick pure Ni as interlayer to join 2-mm AZ31B Mg alloy and 2-mm 5754 Al alloy, higher welding current (32–36 kA) was applied. Furthermore, the electrode tip faces were flattened (with smaller tip face on the Al side) in order to improve the heat balance. The Ni interlayer remained solid and unmelted, preventing the formation of Al-Mg IMCs. Continuous submicron Mg-Ni and Al-Ni intermetallic layers were observed at the Mg/Ni and Al/Ni interfaces, respectively. Consequently, a strong metallurgical joint with an average peak load of about 5.1 kN was obtained [128].

The feasibility of using Zn-based interlayers to join Al to Mg alloys was also studied [126, 129]. 0.25-mm pure Zn foil and 0.7-mm-thick Zn-coated HSLA steel were employed as interlayers to join 2-mm AZ31B Mg alloy to 2-mm Al Alloy 5754. The pure Zn foil led to the formation of brittle IMCs with microhardness values of 224–304 HV in the nugget zone because of the mixing of Al, Mg, and Zn and consequently poor joint. On the other hand, the Zn-coated steel remained unmelted and successfully prevented the mixing of Al and Mg, thereby restricting the formation of brittle IMCs. A joint with a strength of about 3.86 kN was obtained, which is approximately 74 % of the strength of optimized AZ31B/AZ31B spot weld and acceptable as per AWS D17.2 standard [129]. As observed by Penner et al. [129], the application of pure Zn as interlayer to join Al to Mg alloys resulted in poor joint strength. Therefore, in a more recent study [126], a new technique, called thermo-compensated RSW process was proposed and applied to join 1.5-mm AZ31B Mg alloy to 1.5-mm AA5052-H12 Al alloy using 0.4-mm-thick pure Zn as interlayer. In this technique, a 0.5-mm thick AISI 201 stainless tape was inserted between the Al sheet and the upper electrode. More heat was generated in the stainless tape than in the Al alloy because of its lower thermal conductivity and higher electrical resistivity. Thus, the stainless steel acted both as an additional heat source to Al alloy and also as a barrier to restrain heat loss from the nugget. Therefore, there was an increased dissolution of elemental Al into the liquid nugget during the RSW process. As a result of this, the nugget contained large amounts of dissolved Al and Zn-based solid solution, which led to improvement in joint strength. The average peak load of the joint obtained by this technique was found to be 2.2 kN, while that of the joint obtained by conventional RSW was found 0.73 kN [126]. In the most recent study [8], 0.6-mm-thick Sn-coated steel interlayer was found to successfully prevent the formation of brittle of Al-Mg IMCs during RSW of 2-mm AA5052 Al alloy to 2-mm AZ31 Mg

alloy, producing a joint with a maximum tensile shear load of 4.4 kN [8].

Table 3 compares the strengths of Al/Mg dissimilar resistance spot welds, obtained using different interlayers and techniques. From the table, it can be observed that, generally, pure Zn interlayer could not improve the joint strength. Although the thermo-compensated RSW technique resulted in appreciable improvement of Al/Mg dissimilar resistance spot welds using pure Zn interlayer, the joint strength is still low compared to the use of other interlayers. The employment of pure Ni at high welding current, Au-coated Ni and Sn-coated steel interlayers produced the most successful results. However, the application of materials with high cost material is commercially difficult. Therefore, other lower cost and more available interlayers are needed [129]. Thus, there is a need to test other interlayers and the feasibility of applying the thermo-compensated RSW technique with other interlayers also be explored.

10.3 RSW of Al/Ti Alloys

Ti and its alloys are one of the most attractive engineering materials in industrial applications. They possess superior properties, such as high specific strength, high fatigue life, toughness, excellent corrosion resistance. However, its application is limited by its high cost [130]. Joining Ti to other alloys would enhance cost-effectiveness and extend its applications. In particular, Al/Ti hybrid components attract great attention because of their high specific strength, excellent resistance to corrosion [69]. However, joining Al to Ti is difficult due to large differences in physical and thermal properties and formation of brittle IMCs at the interface. So far, very few research has been conducted on Al/Ti dissimilar RSW [69, 130]. Li et al. [68, 69] have joined 2-mm 6061-T6 Al alloy and 1-mm TA1 pure Ti alloy by RSW, with and without EMS. As shown in Fig. 28, the joint is an especial brazed joint. The Al alloy melted while the Ti remained solid (welding-brazing), forming the nugget in the Al alloy. A PMZ is observed at the nugget edge and a CGZ next to it. However, equiaxed crystal zone, which is formed in the interior of the nugget of Al/Al joint was not observed. This is because the Ti sheet restrained the heat loss and lowered the cooling rate, finally interrupting the CET. Thus, a transition structure was observed in the interior of the nugget (Fig. 28c) [68]. Under the influence of EMS, the weld nugget became wider and thinner due to centrifugal motion of the molten metal, which would promote nugget growth in the radial direction (Fig. 31e). The PMZ became wider and CGZ narrower. Furthermore, as shown in Fig. 28g, the EMS effectively refined the microstructure at the interior of the nugget into a nearly spheroidal grains, and thus, this zone is referred to as spheroidal grain zone (SGZ) [68]. As shown in Fig. 28d, h, no visible reaction layer was observed at the Al/Ti interface. This suggested that the thickness of any present IMC layer is less than 1 μm [68]. For the joint produced by conventional RSW, the bonding diameter, peak load, and energy absorption increased with increase in welding current below 16 kA. An average peak load of about 0.7, 2.1, 2.7, 3.5, and 4.22 kN was obtained at welding current of 6, 8, 10, 12, and 14 kA. Furthermore, it was found that at a critical welding current of 16 kA, the joint quality became unstable. This is due to the change of welding mode from welding-brazing to fusion welding (a reaction between liquid aluminum and liquid titanium) mode, which promoted the formation of brittle IMCs, possibly $TiAl_3$, $TiAl_2$, and Ti_5Al_{11}, or a mixture thereof [68, 69]. However, Under EMS, the weld quality improved at all welding currents. Relative to that of the joint produced by conventional RSW, the average peak load increased by 141.1, 19.7, 12.4, 20.2, 26.7, and 29 %, at welding currents of 6, 8, 10, 12, 14, and 16 % respectively. The maximum average peak load of 5.5 kN was obtained at a welding current of 16 kN [68]. Qiu et al. [130] used the technique of RSW with cover plates to join 1-mm A 5052 Al alloy and 1-mm pure Ti. A thin, 160 nm, reaction layer of Al solid solution, supersaturated with Ti and containing precipitates of $TiAl_3$ was observed at the interface. Maximum tensile shear load of 6.4 kN was obtained at 10 kA [130]

Table 3 Strengths of dissimilar Al/Mg resistance spot welds obtained using different techniques, with and without interlayers

Materials	Process	Interlayer	Joint strength (kN)	Reference
2-mm AZ31B Mg alloy/ 2-mm 5754 Al alloy	Conventional RSW	0.2-mm pure nickel	Metallurgical bond not produced	[127]
		0.2-mm pure nickel	5.1	[128]
		0.2-mm gold-coated nickel foil	4.69	[127]
		0.7-mm zinc-coated HSLA steel	3.86	[129]
2-mm AA5052-H32/2-mm AZ31-H24	Conventional RSW	0.6-mm Sn-coated AISI 1008 steel	4.4	[8]
1.5-mm AZ31B Mg alloy/1.5-mm AA5052-H12 Al alloy	Conventional RSW	0.4-mm zinc interlayer	0.73	[126]
	Thermo-compensated RSW	0.4-mm zinc interlayer	2.2	[126]
	Conventional RSW	No interlayer	0.83	[126]

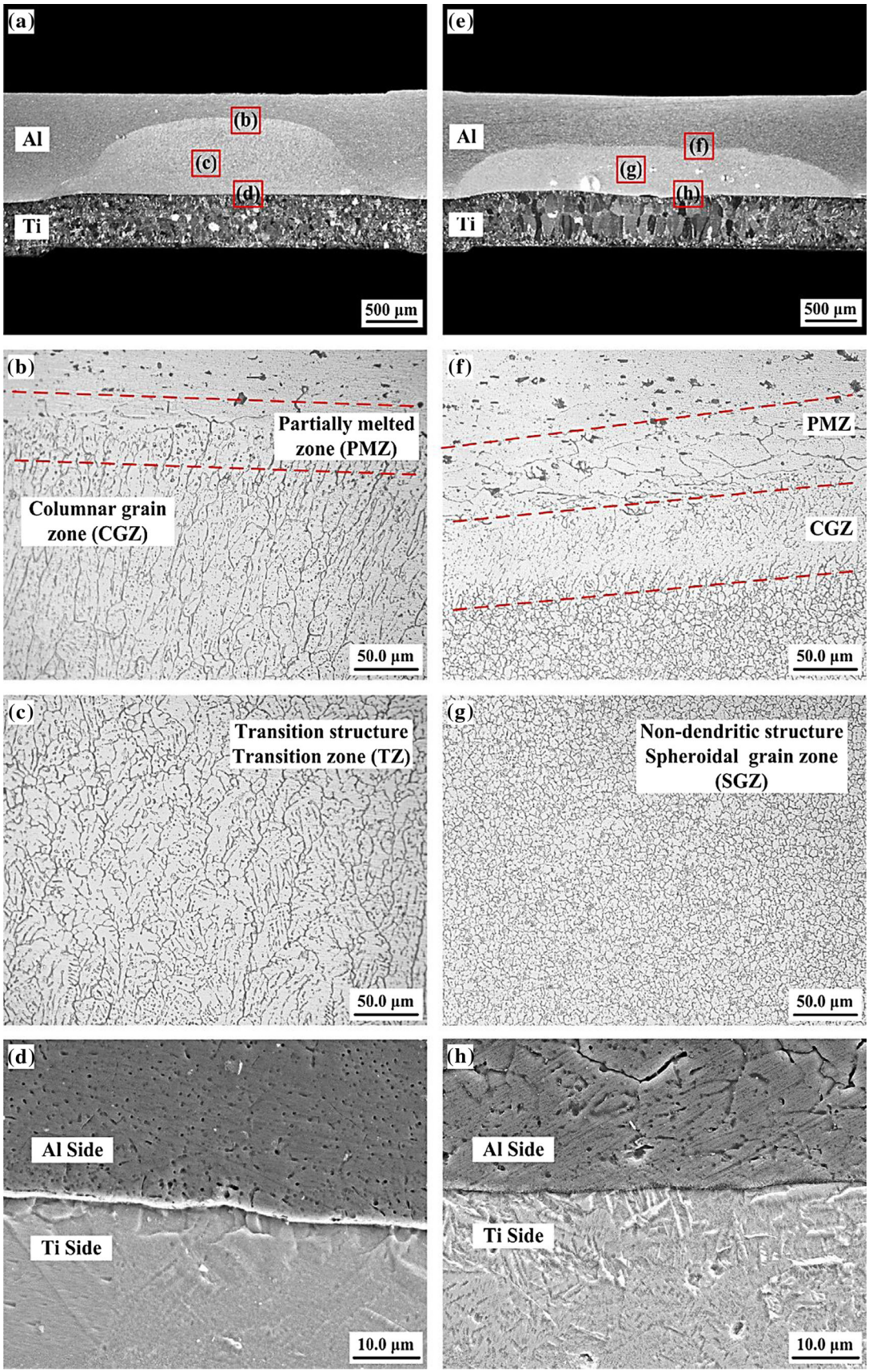

Fig. 28 Microstructure of the Al/Ti resistance spot weld: **a**–**d** Conventional RSW and **e**–**h** RSW with EMS [68]

11 Weld bonding

Adhesive bonding is a cheap, fast, and robust joining technique that is used widely in the automotive, aerospace, nuclear, electronics, and electrical industries. The process is also used in combination with others processes such as RSW, riveting, or mechanical fasteners in order to maximize the benefits of the processes involved [131]. Weld bonding is an innovative and advanced hybrid joining technology which combines the advantages of RSW and adhesive bonding. It is now widely used in automobile, railway carriages, and aircraft manufacturing industries [132, 133]. It produces more desirable joints than either spot welding or adhesive bonding. In addition to reducing the number of welds required in a vehicle, it offers advantages such as reduced manufacturing costs, enhanced stress distribution, fatigue resistance, crashworthiness, corrosion resistance, elimination of the need for sealants, improved stiffness, and load-bearing capacity [60, 133–139]. In the process, structural adhesives are applied on the surface of the sheets followed by RSW and then curing at a suitable temperature for a specific period of time [67, 135, 136].

Surface pre-treatment was found to have strong influence on the properties of adhesive joints. Pereira et al. [131] studied the influence of manufacturing parameters such as surface pre-treatment, adherend thickness (ta), and overlap length (Ls), on the strength of 6082-T6 Al alloy adhesive joints, produced using a two-component, high-strength epoxy adhesive (Araldite 420 A/B). Five different surface pre-treatments were used: cleaning with acetone (SW), caustic etch (CE), sodium dichromate-sulphuric acid etch (CSA), Tucker's reagent etch (TR), and abrasive polishing (AP). As shown in Fig. 29, CSA produced the best result followed by (AP). The highest strength obtained by CSA is attributed to lower surface roughness, which would result in a smaller angle of contact. The failure load was also found to increase significantly with increased Ls.

Khan and Dwivedi [65] studied the mechanical and metallurgical behavior of weld-bonded 2-mm 6061-T6 Al alloy, produced using 2-C plain epoxy resin adhesive (cured at 120 °C for 60 min). A corona bond zone was observed in the HAZ, close to the nugget, where the adhesive layer was displaced. Furthermore, the welding thermal cycle damaged a thin band of the adhesive around the circumference of the spot. Under cyclic loadings, fracture in both the spot welds and weld bonds mostly initiated from circumferential zone of nugget. However, the presence of adhesive lowers the stress concentration and thus improved the fatigue life of the weld-bonded joint. The fatigue life of the weld-bonded joint was found to be approximately 0.62×10^6 cycles, which is significantly higher than that of adhesive bonded joint (about 22,000 cycles) and that of the resistance spot weld (1000 cycles) [65]. In another study, fatigue tests were conducted on series of resistance spot welds and weld bonds of 1-mm 6082-T6 Al alloy. The weld-bonding was conducted with two different sets of welding parameters, named F5 (2.65 kN, 3 cycles, and 26.4 kA) and F6 (3.24 kN, 2 cycles, and 26.9 kA) using a high strength, two-component epoxy adhesive (Araldite 420 A/B, cured at 50 °C for 4 h). As shown in Fig. 30, the fatigue strength of weld-bonded specimens was found to be significantly higher than that of the resistance spot welds. Furthermore, the fatigue resistance of the two weld bonds (F5 and F6) was found to be similar, suggesting that the little variation in welding parameters had insignificant effect on the fatigue strength of the weld-bonded joints [89].

The quasi-static tensile shear load of weld-bonded bonds of Al alloys is also higher than that of spot welds. The introduction of insulating adhesive increases the contact resistance and thus heat generation, resulting in enlarged nugget size.

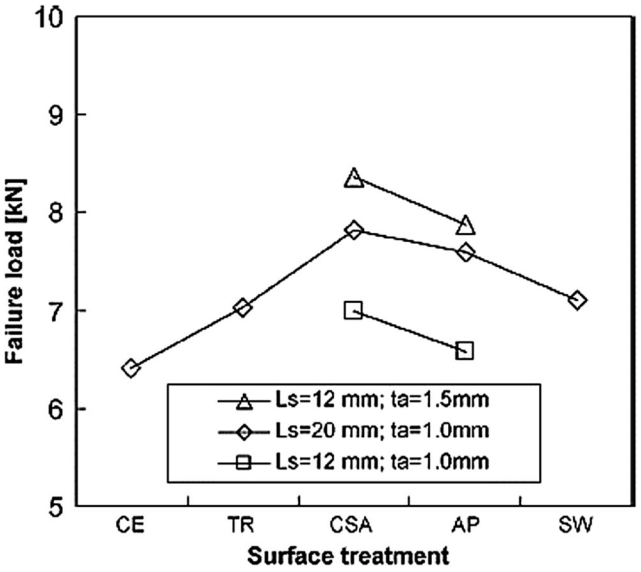

Fig. 29 Failure load of 6082-T6 Al alloy adhesive bonds as a function of the surface preparation, adherend thickness, and overlap length [131]

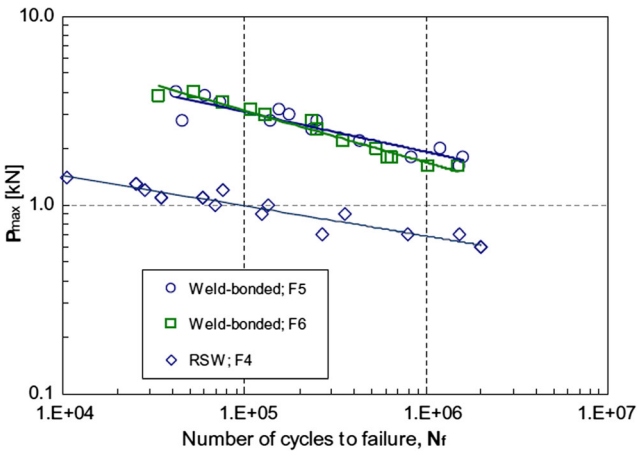

Fig. 30 Fatigue behavior of weld-bonded and RSW 1-mm 6082-T6 Al alloy [89]

However, the risk of expulsion is also higher in weld bonding [65, 67]. Khan et al. [60] developed a response surface model to study the influence of significant process parameters (welding current (C), welding time (T), and welding pressure (P)) and their interactions (welding current-welding time (CT), welding current-welding pressure (CP), and welding time-welding pressure (TP)) on the tensile shear strength (TS) of weld-bonded 2-mm AA 6061-T6 Al alloy, produced using 2-C Plain Epoxy Resin adhesive (cured at 120 °C for 60 min). The CT interaction was found to have more significant effect on the strength than that of CP and TP. The strength increased with increase in welding current and welding time up to a certain level and then decreased with further increase in these parameters due to excessive heat generation, which caused expulsion and damage to the adhesive. Thus, the welding parameters should be carefully selected [60].

12 Main metallurgical defects in RSW of Al alloys

12.1 Expulsion

Expulsion (the ejection of molten metal from the nugget area) is a common phenomenon in RSW. It occurs either at the electrode/workpiece interface (surface expulsion) or at the faying surface (interfacial expulsion), mainly due to the application of high welding current for a short period of time [51, 82, 106, 107, 140, 141]. Surface expulsion may severely affect surface quality and electrode life but not the strength. On the other hand, interfacial expulsion may affect the strength of the joint due to loss of liquid metal from the nugget, making it highly undesirable [51, 82], particularly in weld bonding, where the integrity of the bond line may be compromised [23]. Heavy expulsion can produce large cavity in the nugget due to volume deficit [82].

The risk of expulsion is particularly high in RSW of Al alloys, due to the presence of oxide layer and the need for high welding current for a short period time [25, 82]. Senkara et al. [82] analyzed the forces involved in RSW and developed a criterion for interfacial expulsion, which was verified by experiments on A 5754 Al alloy. The criterion is that "Expulsion occurs when the force from the liquid nugget onto its solid containment equals or exceeds the effective electrode force" [82]. The most significant factor that induces expulsion is the welding current, followed by electrode force [142]. Thus, enhancing electrode force is beneficial in suppressing expulsion.

12.2 Porosity

Pore formation in RSW is caused by factors such as surface contamination, hydrogen rejection during solidification, pre-existing pores in the BM, shrinkage strain, and expulsion [79, 143, 144]. Porosity has been observed in the FZ of Al alloy resistance spot welds [21, 36, 77, 85, 140]. For example, large porosities, approximately 60 μm in diameter, were observed in fracture surface of 2-mm 6061-T6 Al alloy resistance spot weld [36]. Similarly, Gean et al. [85] observed substantial porosity in the nugget of 1.2-mm 5182-0 Al alloy, especially in samples welded with low electrode force[85]. Figure 31 shows some defects, including porosity, in the nugget of AA6022-T4 spot weld, produced at a welding current of 31 kA and welding time of 133 ms [77]. It has been reported that porosity decreases with increased electrode force [22, 85]. For example, Hassanifard et al. [22] found that pore fraction (the ratio of porosity or void area to fusion zone area) during RSW of 1.5-mm 5083-O Al alloy decreased from 4.6 to 3.7 to 2.4 % with increase in electrode force from 2.5 to 3 to 3.5 kN, respectively.

12.3 Liquation cracking

Cracking is one of the major concerns in welding Al alloys due to the presence of low melting point eutectics, such as Al-Cu, Al-Mg, and Al-Mg-Si, and also due to high solidification shrinkage and large coefficient of thermal expansion [51, 140, 145]. During RSW of Al alloys, the formation of liquid films around grains in the HAZ due to constitutional melting of the alloy and liquation of secondary phases provide favorable conditions for cracking [140, 145]. Senkara and Zhang [140] studied liquation cracking in RSW of AA5754 Al alloy. Although some porosity was observed in the nugget of the samples, no cracks were observed in the nuggets. However, many cracks were observed in the HAZ of many samples. As shown in Fig. 32, the cracks initiated close to weld interface in the HAZ, where the alloy remained in the solidus-liquidus temperature range during welding. The cracks then propagated into the BM. As shown in the figure, most of the cracks are

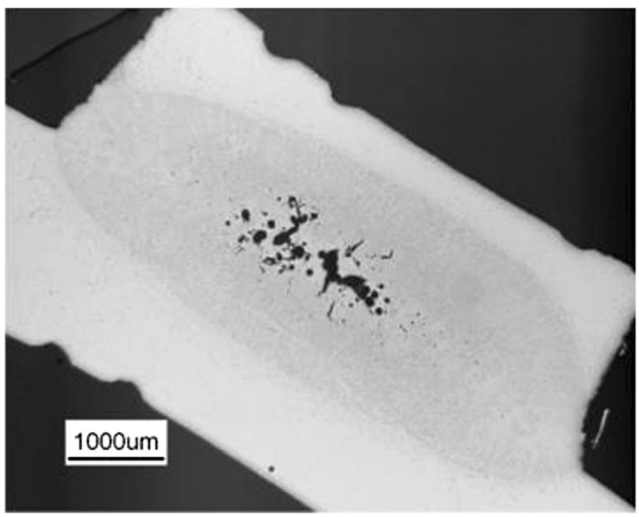

Fig. 31 Microstructure of AA6022-T4 spot weld [77]

wider at their bases and became narrower towards the BM, with fairly repeatable appearance and orientation. A thermomechanical analysis revealed that tensile stresses have built up on the cracked side of the joint due to material flow, thermal stress development, and localized straining [140].

13 Electrode degradation

Rapid electrode tip wear is one of the major problems in RSW of Al alloys due to the presence of oxide layer and usage of high welding current [16, 42–44, 59, 146–148]. A study of the electrode life during RSW of 1.5-mm 5182 Al alloy has shown that the electrode life was in the range of about 400 to 900 welds. Electrode degradation was found to increase the contact area at the electrode/sheet interface, thus reducing the current density, leading to an undersized nugget [31]

Lum et al. [146] found, while studying the electrode degradation mechanism during RSW of 5182 Al alloy, that the degradation occurred in four basic steps, namely, Al pickup, alloying of electrode with Al, electrode tip face pitting, and cavitation. Al pickup begins right from the first weld as tiny drops of molten Al are transferred from the sheet surface to the electrode tip face. This molten Al adheres to and reacts with the electrode, forming of complex Cu-Al alloys (mainly $CuAl_2$ and traces of Cu_9Al_4). The Cu-Al mixture breaks up and as a result, pitting (material loss from the tip face) occurs, initially on a ring near the periphery of the contact zone, where the highest surface temperature is attained. Finally, smaller pits grow and combine together to form large cavities [146].

Electrode degradation was found to be more significant on top electrodes than on bottom electrodes due to Peltier effect (top electrode positive and bottom electrode negative), which results in higher heat generation at the top electrode [146]. The cost of redressing or replacing the electrodes and the shut-down times affect production cost and efficiency [27]. Thus, it is important to improve electrode life. It was found that periodic cleaning of the electrode would limit Al pickup and thus extend the electrode life (Fig. 33) [146]. Furthermore, Rashid et al. [59] proposed the application of a thin layer of lubricant at the electrode/workpiece interface to influence the electrode life. RSW of AA5182 Al alloy was investigated using different metalworking lubricants. For the same welding conditions, one of the lubricants was found to extend the electrode life to 730 welds, which was almost double the electrode life for the unlubricated surface. The lubricant thinned the surface oxide layer and thus reduced the heat generation which led to reduced alloying and pitting rate. However, other lubricants showed negative effect on electrode degradation. Thus, further study is needed to find the exact mechanism and to develop suitable lubricants.

14 Future trend

So far, quite a lot of research has been conducted on RSW of Al alloys. However, compared to that of steel, the RSW of Al

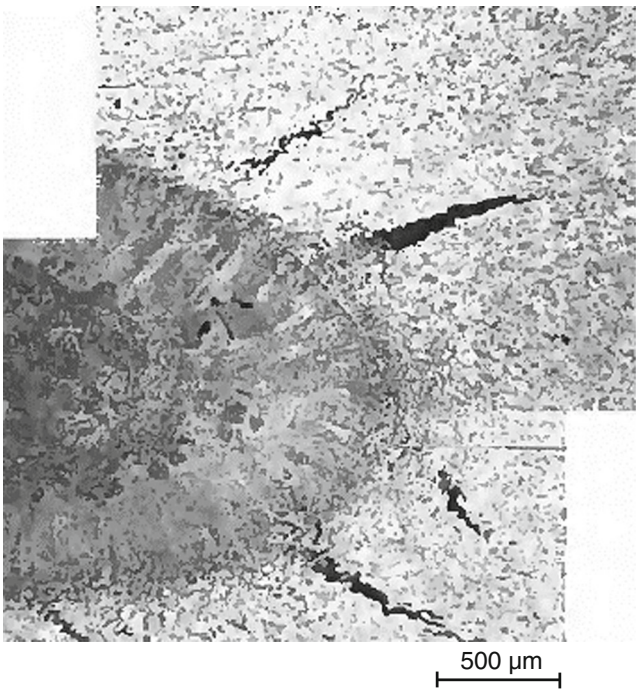

Fig. 32 Liquation cracks in the HAZ of AA5754 Al alloy [140] spot weld

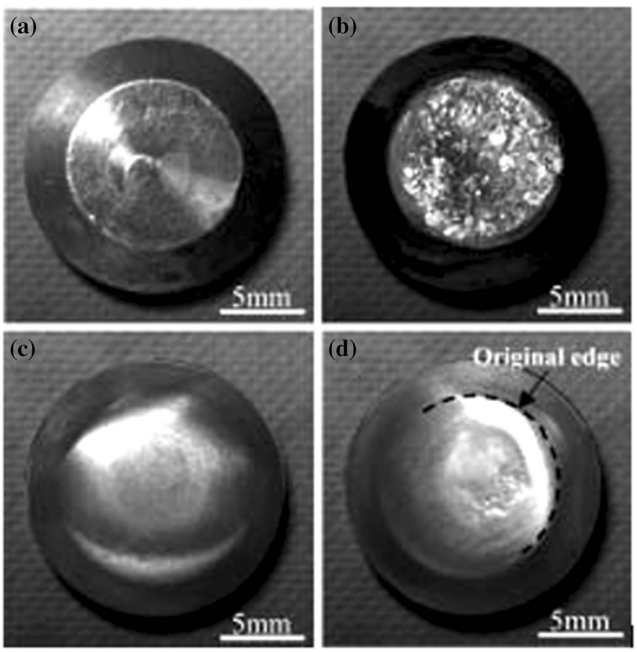

Fig. 33 Appearances of **a** a new electrode and used electrodes after 2000 welds; **b** without periodic cleaning; **c** with cleaning every 20 welds; and **d** with cleaning every 50 welds during RSW of 5182 Al alloy [146]

alloys is in a less advanced stage. Most of the research conducted focused on 5xxx and 6 xxx series Al alloys. Little work has been done on RSW of 7xxx series, which also have wide range of applications in the automotive industry but limited weldability. To fully incorporate Al alloys into the automotive and aerospace structures, there is a need to explore the weldability of different series of Al alloys, both in similar and dissimilar combinations with one another. The newly developed RPW, which appears to be promising in welding 7xxxx alloys should be further explored, for example, by optimizing the compositions and dimensions of the filler rod.

As pointed out in this paper, the oxide layer on the surface of Al alloys presents difficulties, such as high heat generation and rapid electrode tip wear, during RSW. Thus far, both mechanical and chemical means have been used to remove or reduce this oxide layer. It would be of great importance to conduct a thorough research to compare the effectiveness of these two methods, in terms of remaining oxide layer thickness, contact resistance, surface roughness, electrode degradation, range of usable welding parameters, and joint mechanical performance.

Currently, steel is the main structural material in the automotive industry. Joining Al to steels has been challenging due to the wide differences in physical and metallurgical properties. Since the use of some interlayers was found to be beneficial in welding Al to steel, it is important to develop and test other interlayers and also to combine the use of interlayers with other successful techniques such as RSW with cover plates and RSW with optimized electrode morphology. Furthermore, the technique of REW, which seems promising should also be further studied and also applied to other Al/steel combinations. New advanced high strength steels, such as transformation induced plasticity steels and twinning induced plasticity steels, are being developed. It is therefore imperative to study the weldability of these steels to various series of Al alloys.

For Al/Mg dissimilar RSW, the employment of some interlayers has proven effective in restraining the formation of brittle IMCs, with the most successful results obtained, so far, using pure Ni foil, Au-coated Ni foil, and Sn-coated interlayers. Other interlayers, with lower cost and more availability should be developed and tested. It would also be useful to study the feasibility of combining thermo-compensated RSW technique with other interlayers. Extremely limited study has been conducted on Al/Ti joints. The weldability of this important materials combination should be explored in details. The possibility of using interlayers for such dissimilar materials combination should also be explored, due to their tendency to prevent formation of IMCs when properly selected.

Fatigue is the major structural failure, especially in resistance spot-welded joints. Little study has been reported on fatigue behavior of Al/Al alloys and Al alloys/steel resistance spot welds, and no study has been reported on fatigue behavior of Al/Mg and Al/Ti dissimilar resistance spot welds. To guarantee the light-weighting and crashworthiness of automotive structures, such studies should be conducted. The weld bonding technology has proven to be beneficial in enhancing fatigue behavior of spot welds. It should be studied extensively and also applied during RSW of Al/Mg, Al/Ti, and Al/steel dissimilar joints

Electrode degradation is a major concern in RSW of Al alloys. One study has shown that the use some lubricants can extend the electrode life, while other lubricants have negative effect on electrode degradation. Thus, it is important to understand the exact mechanism and to develop suitable lubricants.

Finally, despite the importance of corrosion to the life of automobiles, no study has been conducted on the effect of RSW on the corrosion behavior of Al spot welds. Such study is crucial and should be undertaken.

15 Summary

Fuel consumption and greenhouse gas emissions have been attracting global concern. The transportation industry has been exploiting many strategies to improve fuel efficiency, of which weight reduction is the most cost-effective. With a low density, one third the density of steel, and high specific strength, Al alloys have great potentials for weight savings and are increasingly being incorporated into the automotive and aerospace structures. On the other hand, RSW is the most popular sheet joining process, especially in the automotive industry. This paper presents a review on RSW of Al/Al alloys, Al/steel, Al/Mg, Al/Ti alloys, and weld bonding, with emphasis on structure, properties, and performance relationships, under quasi-static and dynamic loading conditions.

The RSW of Al alloys present some difficulties. The presence of non-conducting, tenacious, and refractory oxide layer on the surface of Al alloys induces high contact resistance at both the electrode/workpiece and faying interface. Furthermore, due to their high thermal conductivity, high welding current, typically two to three times for steel, is required in RSW of Al alloys. These lead to rapid electrode tip wear and associated inconsistency in weld. It has been shown that cleaning the oxide layer, either mechanically or chemically, leads to significant reduction in contact resistance and improvement of joint quality. It has also been shown that small relative rotation or sliding between sheets, increasing the electrode force, and applying a low-current preheat are beneficial in reducing the contact resistance.

The microstructure of Al resistance spot welds usually consists of ECZ at the interior of the nugget and CDZ at the edge of the nugget. RSW under the influence of EMS results in microstructure refinement of both the EDZ and CDZ and also

increases the proportion of equiaxed grains, thus improving mechanical properties. A significant reduction in hardness is normally observed in the FZ and HZ of spot welds in heat treatable, 6xxx series Al alloys, especially in the T6 state, due to the dissolution of hardening precipitates. The reduction in hardness is concentrated mainly in the nugget center, because it experiences the highest temperature.

During TS shear test, resistance spot welds of Al alloys commonly fail in IF mode partly because the hardness in the FZ is less than or comparable to that of the BM. It was found that for any sheet stacks, the strength of Al spot welds in TS, CT, and CP configurations is governed by the smallest sheet thickness (GMT), as it has the lowest tearing resistance. As GMT increases, the strengths also increase. The fatigue behavior of Al alloys is similar to that of Mg alloys but significantly less than that of steels. In LCF regime, Mg and Al alloys spot welds, in TS configuration, fail in IF mode, while those of steel fail from the HAZ due higher strength in the FZ. In the HCF, steel, Mg and Al alloys spot welds commonly fail in coupon failure mode. Residual stresses, which may be as high as the yield strength of the BM, are formed in the nugget of Al spot welds, with highest value obtained at the center of the nugget. Increasing electrode force is useful in reducing residual stresses and also improving fatigue life.

Weld bonding, which combines adhesive bonding and RSW, was found to significantly improve the quasi-static and fatigue behavior of spot welds. However, the welding parameters should be carefully selected to avoid expulsion and poor joint quality.

Due to differences in physical and thermal properties dissimilar RSW between Al/steel, Al/Mg, and Al/Ti alloys lead to the formation of brittle IMCs which could impair the joint quality. For Al/steel dissimilar RSW, the technique of resistance element welding, the use of optimized electrode morphology, the technique of RSW with cover plates, and the use of interlayers such as Al-Mg, AlSi12, and AlCu28 alloys were found to suppress the formation of brittle IMCs and improve the joint quality. The employment of pure Ni foil, Au-coated Ni foil, Sn-coated steel, and Zn-coated steel interlayers was also found to restrict the formation of brittle IMCs during RSW of Al/Mg alloys. The techniques of RSW with cover plates and RSW under the influence of electromagnetic stirring effect improve the weldability of the joints of Al/Ti dissimilar joints.

RSW parameters, especially welding current, welding time, and electrode force, strongly influence the quality and performance of Al spot welds. Because of the high thermal conductivity and low electrical resistivity of Al alloys, high welding current and short welding time are needed during RSW of Al alloys. In order to obtain sound joints with desired geometry and mechanical importance, the RSW parameters should be carefully selected and be within certain critical range, so as to avoid excessive expulsion, unacceptable electrode indentation, and poor joint quality.

Electrode degradation is a major concern in RSW of Al alloys. It occurs in four basic steps, namely, Al pickup, alloying of electrode with Al, electrode tip face pitting, and cavitation. Periodic cleaning of the electrodes and the application of a thin layer of suitable lubricants at the electrode/workpiece interface are beneficial in extending the electrode life.

Acknowledgments The authors would like to acknowledge University of Malaya for providing the necessary facilities and resources for this research. This research was supported by University of Malaya Research Grant (UMRG) (RP035A-15AET)

References

1. Kim HC, Wallington TJ (2013) Life-cycle energy and greenhouse gas emission benefits of lightweighting in automobiles: review and harmonization. Environ Sci Technol 47(12):6089–6097
2. Humpenöder F, Popp A, Stevanovic M, Müller C, Bodirsky BL, Bonsch M, Dietrich JP, Lotze-Campen H, Weindl I, Biewald A (2015) Land-use and carbon cycle responses to moderate climate change: implications for land-based mitigation? Environ Sci Technol
3. Modaresi R, Pauliuk S, Løvik AN, Müller DB (2014) Global carbon benefits of material substitution in passenger cars until 2050 and the impact on the steel and aluminum industries. Environ Sci Technol 48(18):10776–10784
4. Das S (2014) Life cycle energy and environmental assessment of aluminum-intensive vehicle design. SAE Int J Mater Manuf 7(2014-01-1004):588–595
5. Kulekci MK (2008) Magnesium and its alloys applications in automotive industry. Int J Adv Manuf Technol 39(9-10):851–865
6. Medraj M, Parvez A (2007) Analyse the importance of magnesium-aluminium-strontium alloys for more fuel-efficient automobiles. Automotive:45–47
7. Association EA (2008) Aluminium in cars. European Aluminium Association
8. Sun M, Niknejad S, Gao H, Wu L, Zhou Y (2016) Mechanical properties of dissimilar resistance spot welds of aluminum to magnesium with Sn-coated steel interlayer. Mater Des 91:331–339
9. Ambroziak A, Korzeniowski M (2010) Using resistance spot welding for joining aluminium elements in automotive industry. Arch Civ Mech Eng 10(1):5–13
10. Automotive Trends in Aluminum, The European perspective: part one. http://www.totalmateria.com/Article135.htm Accessed 12 Dec 2015
11. Rodriguez R, Jordon J, Allison P, Rushing T, Garcia L (2015) Microstructure and mechanical properties of dissimilar friction stir welding of 6061-to-7050 aluminum alloys. Mater Des 83:60–65
12. Liu J, Rao Z, Liao S, Wang P-C (2014) Modeling of transport phenomena and solidification cracking in laser spot bead-on-plate welding of AA6063-T6 alloy. Part I—the mathematical model. Int J Adv Manuf Technol 73(9-12):1705–1716
13. Qiu R, Zhang Z, Zhang K, Shi H, Ding G (2011) Influence of welding parameters on the tensile shear strength of aluminum alloy joint welded by resistance spot welding. J Mater Eng Perform 20(3):355–358
14. Karimi M, Sedighi M, Afshari D (2015) Thermal contact conductance effect in modeling of resistance spot welding process of

aluminum alloy 6061-T6. Int J Adv Manuf Technol 77(5-8):885–895
15. Han L, Thornton M, Shergold M (2010) A comparison of the mechanical behaviour of self-piercing riveted and resistance spot welded aluminium sheets for the automotive industry. Mater Des 31(3):1457–1467
16. Han L, Thornton M, Li D, Shergold M (2011) Effect of governing metal thickness and stack orientation on weld quality and mechanical behaviour of resistance spot welding of AA5754 aluminium. Mater Des 32(4):2107–2114
17. Zhang Y, Li Y, Luo Z, Yuan T, Bi J, Wang ZM, Wang ZP, Chao YJ (2016) Feasibility study of dissimilar joining of aluminum alloy 5052 to pure copper via thermo-compensated resistance spot welding. Mater Des 106:235–246
18. Shi Y, Guo H (2013) Fatigue performance and fatigue damage parameter estimation of spot welded joints of aluminium alloys 6111-T4 and 5754. Fatigue Fract Eng Mater Struct 36(10):1081–1090
19. Wu S-n, Ghaffari B, Hetrick E, Li M, Z-h J, Liu Q (2014) Microstructure characterization and quasi-static failure behavior of resistance spot welds of AA6111-T4 aluminum alloy. Trans Nonferrous Metals Soc China 24(12):3879–3885
20. Miller W, Zhuang L, Bottema J, Wittebrood AJ, De Smet P, Haszler A, Vieregge A (2000) Recent development in aluminium alloys for the automotive industry. Mater Sci Eng A 280(1):37–49
21. Feng Y, Luo Z, Li Y, Ling Z (2016) A novel method for resistance plug welding of 7075 aluminum alloy. Mater Manuf Process:1–7. doi:10.1080/10426914.2015.1103853
22. Hassanifard S, Zehsaz M, Tohgo K (2011) The effects of electrode force on the mechanical behaviour of resistance spot-welded 5083-O aluminium alloy joints. Strain 47(s1):e196–e204
23. Hao M, Osman K, Boomer D, Newton C (1996) Developments in characterization of resistance spot welding of aluminum. Weld J Incl Weld Res Suppl 75(1):1–4
24. Cho Y, Hu S, Li W (2003) Resistance spot welding of aluminium and steel: a comparative experimental study. Proc Inst Mech Eng B J Eng Manuf 217(10):1355–1363
25. Luo Z, Ao S, Chao YJ, Cui X, Li Y, Lin Y (2015) Application of pre-heating to improve the consistency and quality in AA5052 resistance spot welding. J Mater Eng Perform 24(10):3881–3891
26. Cui LH, Qiu RF, Shi HX, Zhu YM (2014) Resistance spot welding between copper coated steel and aluminum alloy. Appl Mech Mater 675:19–22
27. Florea R, Solanki K, Bammann D, Baird J, Jordon J, Castanier M (2012) Resistance spot welding of 6061-T6 aluminum: failure loads and deformation. Mater Des 34:624–630
28. 2015 North American light vehicle aluminum content study: executive summary http://www.drivealuminum.org/research-resources/PDF/Research/2014/2014-ducker-report. Accessed 12 Dec 2015
29. Wang J, Wang H-P, Lu F, Carlson BE, Sigler DR (2015) Analysis of Al-steel resistance spot welding process by developing a fully coupled multi-physics simulation model. Int J Heat Mass Transf 89:1061–1072
30. Li Y, Luo Z, Yan FY, Duan R, Yao Q (2014) Effect of external magnetic field on resistance spot welds of aluminum alloy. Mater Des 56:1025–1033
31. Fukumoto S, Lum I, Biro E, Boomer D, Zhou Y (2003) Effects of electrode degradation on electrode life in resistance spot welding of aluminum alloy 5182. Weld J 82(11):307-S
32. Bi J, Song J, Wei Q, Zhang Y, Li Y, Luo Z (2016) Characteristics of shunting in resistance spot welding for dissimilar unequal-thickness aluminum alloys under large thickness ratio. Mater Des 101:226–235
33. Li YB, Wei ZY, Li YT, Shen Q, Lin ZQ (2013) Effects of cone angle of truncated electrode on heat and mass transfer in resistance spot welding. Int J Heat Mass Transf 65:400–408
34. Hamidinejad SM, Kolahan F, Kokabi AH (2012) The modeling and process analysis of resistance spot welding on galvanized steel sheets used in car body manufacturing. Mater Des 34:759–767
35. Hayat F (2011) The effects of the welding current on heat input, nugget geometry, and the mechanical and fractural properties of resistance spot welding on Mg/Al dissimilar materials. Mater Des 32(4):2476–2484
36. Florea R, Bammann D, Yeldell A, Solanki K, Hammi Y (2013) Welding parameters influence on fatigue life and microstructure in resistance spot welding of 6061-T6 aluminum alloy. Mater Des 45:456–465
37. Pouranvari M, Marashi S (2013) Critical review of automotive steels spot welding: process, structure and properties. Sci Technol Weld Join 18(5):361–403
38. Manladan S, Yusof F, Ramesh S, Fadzil M (2016) A review on resistance spot welding of magnesium alloys. Int J Adv Manuf Technol:1-21. doi: 10.1007/s00170-015-8258-9
39. Satonaka S, Iwamoto C, Murakami GI, Matsumoto Y (2012) Resistance spot welding of magnesium alloy sheets with cover plates. Weld World 56(7-8):44–50
40. Al Naimi IK, Al Saadi MH, Daws KM, Bay N (2015) Influence of surface pretreatment in resistance spot welding of aluminum AA1050. Prod Manuf Res 3(1):185–200
41. Florea R, Hubbard C, Solanki K, Bammann D, Whittington W, Marin E (2012) Quantifying residual stresses in resistance spot welding of 6061-T6 aluminum alloy sheets via neutron diffraction measurements. J Mater Process Technol 212(11):2358–2370
42. Rashid M (2011) Some tribological influences on the electrode-worksheet interface during resistance spot welding of aluminum alloys. J Mater Eng Perform 20(3):456–462
43. Patil R, Anurag Tilak C, Srivastava V, De A (2011) Minimising electrode wear in resistance spot welding of aluminium alloys. Sci Technol Weld Join 16(6):509–513
44. De A (2002) Finite element modelling of resistance spot welding of aluminium with spherical tip electrodes. Sci Technol Weld Join 7(2):119–124
45. Cho Y, Li W, Hu S (2006) Design of experiment analysis and weld lobe estimation for aluminum resistance spot welding. Weld J 85(3):45–51
46. Wei PS, Wu TH, Chen LJ (2013) Joint quality affected by electrode contact condition during resistance spot welding. IEEE Trans Compon Pack Manuf Technol 3(12):2164–2173
47. Liu L, Feng J, Zhou Y (2010) 18 - Resistance spot welding of magnesium alloys. In: Liu L (ed) Welding and joining of magnesium alloys. Woodhead Publishing, pp 351–367e
48. Qiu RF, Satonaka S, Iwamoto C (2009) Mechanical properties and microstructures of magnesium alloy AZ31B joint fabricated by resistance spot welding with cover plates. Sci Technol Weld Join 14(8):691–697
49. Charde N, Yusof F, Rajkumar R (2014) Material characterizations of mild steels, stainless steels, and both steel mixed joints under resistance spot welding (2-mm sheets). Int J Adv Manuf Technol 75(1-4):373–384
50. Wang Y, Mo Z, Feng J, Zhang Z (2007) Effect of welding time on microstructure and tensile shear load in resistance spot welded joints of AZ31 Mg alloy. Sci Technol Weld Join 12(8):671–676
51. Zhang H, Senkara J (2011) Resistance welding: fundamentals and applications. CRC Press
52. Williams N, Parker J (2004) Review of resistance spot welding of steel sheets part 1 modelling and control of weld nugget formation. Int Mater Rev 49(2):45–75

53. James P, Chandler H, Evans J, Wen J, Browne D, Newton C (1997) The effect of mechanical loading on the contact resistance of coated aluminium. Mater Sci Eng A 230(1):194–201
54. Crinon E, Evans J (1998) The effect of surface roughness, oxide film thickness and interfacial sliding on the electrical contact resistance of aluminium. Mater Sci Eng A 242(1):121–128
55. Rashid M, Medley J, Zhou Y (2011) Nugget formation and growth during resistance spot welding of aluminium alloy 5182. Can Metall Q 50(1):61–71
56. Han L, Thornton M, Boomer D, Shergold M (2010) Effect of aluminium sheet surface conditions on feasibility and quality of resistance spot welding. J Mater Process Technol 210(8):1076–1082
57. Rashid M, Medley J, Zhou Y (2009) Electrode worksheet interface behaviour during resistance spot welding of Al alloy 5182. Sci Technol Weld Join 14(4):295–304
58. Alliance RWM (2003) Resistance welding manual. RWMA, Philadelphia
59. Rashid M, Fukumoto S, Medley J, Villafuerte J, Zhou Y (2007) Influence of lubricants on electrode life in resistance spot welding of aluminum alloys. Weld J 86(3):62
60. Khan MF, Dwivedi D, Sharma S (2012) Development of response surface model for tensile shear strength of weld-bonds of aluminium alloy 6061 T651. Mater Des 34:673–678
61. Zhang W, Sun D, Han L, Gao W, Qiu X (2011) Characterization of intermetallic compounds in dissimilar material resistance spot welded joint of high strength steel and aluminum alloy. Isij Int 51(11):1870–1877
62. Zhang W, Qiu X, Sun D, Han L (2011) Effects of resistance spot welding parameters on microstructures and mechanical properties of dissimilar material joints of galvanised high strength steel and aluminium alloy. Sci Technol Weld Join 16(2):153–161
63. Pereira A, Ferreira J, Loureiro A, Costa J, Bártolo P (2010) Effect of process parameters on the strength of resistance spot welds in 6082-T6 aluminium alloy. Mater Des 31(5):2454–2463
64. Zhang W, Sun D, Han L, Liu D (2014) Interfacial microstructure and mechanical property of resistance spot welded joint of high strength steel and aluminium alloy with 4047 AlSi12 interlayer. Mater Des 57:186–194
65. Faseeulla Khan M, Dwivedi D (2012) Mechanical and metallurgical behavior of weld-bonds of 6061 aluminum alloy. Mater Manuf Process 27(6):670–675
66. Zhang W, Sun D, Han L, Li Y (2015) Optimised design of electrode morphology for novel dissimilar resistance spot welding of aluminium alloy and galvanised high strength steel. Mater Des 85:461–470
67. Khan MF, Sharma G, Dwivedi D (2015) Weld-bonding of 6061 aluminium alloy. Int J Adv Manuf Technol 78(5-8):863–873
68. Li Y, Zhang Y, Bi J, Luo Z (2015) Impact of electromagnetic stirring upon weld quality of Al/Ti dissimilar materials resistance spot welding. Mater Des 83:577–586
69. Li Y, Zhang Y, Luo Z (2015) Microstructure and mechanical properties of Al/Ti joints welded by resistance spot welding. Sci Technol Weld Join 20(5):385–394
70. Luo Z, Yan F, Li Y, Bai Y, Yao Q, Tan H (2015) Numerical and experimental study on nugget formation process in resistance spot welding of aluminum alloy. Trans Tianjin Univ 21:135–139
71. Li Y, Yan FY, Luo Z, Chao YJ, Ao SS, Cui XT (2015) Weld growth mechanisms and failure behavior of three-sheet resistance spot welds made of 5052 aluminum alloy. J Mater Eng Perform 24(6):2546–2555
72. Wang Y, Feng J, Zhang Z (2006) Microstructure characteristics of resistance spot welds of AZ31 Mg alloy. Sci Technol Weld Join 11(5):555–560
73. Afshari D, Sedighi M, Barsoum Z, Peng RL (2012) An approach in prediction of failure in resistance spot welded aluminum 6061-T6 under quasi-static tensile test. Proc Inst Mech Eng B J Eng Manuf 226(6):1026–1032
74. Xiao L, Liu L, Esmaeili S, Zhou Y (2012) Microstructure refinement after the addition of titanium particles in AZ31 magnesium alloy resistance spot welds. Metall Mater Trans A 43(2):598–609
75. Xiao L, Liu L, Zhou Y, Esmaeili S (2010) Resistance-spot-welded AZ31 magnesium alloys: part I. Dependence of fusion zone microstructures on second-phase particles. Metall Mater Trans A 41(6):1511–1522
76. Liu L, Xiao L, Feng JC, Tian YH, Zhou SQ, Zhou Y (2010) Resistance spot welded AZ31 magnesium alloys, part II: effects of welding current on microstructure and mechanical properties. Metall Mater Trans A 41a(10):2642–2650
77. Kang JD, McDermid JR, Bruhis M (2013) Determination of the constitutive behaviour of AA6022-T4 aluminium alloy spot welds at large strains. Mater Sci Eng a-Struct 567:95–100
78. Hayat F (2012) Effect of aging treatment on the microstructure and mechanical properties of the similar and dissimilar 6061-T6/7075-T651 RSW joints. Mater Sci Eng A 556:834–843
79. Babu NK, Brauser S, Rethmeier M, Cross C (2012) Characterization of microstructure and deformation behaviour of resistance spot welded AZ31 magnesium alloy. Mater Sci Eng A 549:149–156
80. Alizadeh-Sh M, Marashi S, Pouranvari M (2014) Microstructure-properties relationships in martensitic stainless steel resistance spot welds. Sci Technol Weld Join 19(7):595–602
81. Yao Q, Luo Z, Li Y, Yan F, Duan R (2014) Effect of electromagnetic stirring on the microstructures and mechanical properties of magnesium alloy resistance spot weld. Mater Des 63:200–207
82. Senkara J, Zhang H, Hu S (2004) Expulsion prediction in resistance spot welding. Weld J NY 83(4):123-S
83. Han L, Thornton M, Boomer D, Shergold M (2011) A correlation study of mechanical strength of resistance spot welding of AA5754 aluminium alloy. J Mater Process Technol 211(3):513–521
84. Radakovic D, Tumuluru M (2008) Predicting resistance spot weld failure modes in shear tension tests of advanced high-strength automotive steels. Weld J 87(4):96
85. Gean A, Westgate S, Kucza J, Ehrstrom J (1999) Static and fatigue behavior of spot-welded 5182-0 aluminum alloy sheet. Weld J 78:80-s
86. Sun X, Stephens EV, Davies RW, Khaleel M, Spinella DJ (2004) Effects of fusion zone size on failure modes and static strength of aluminum resistance spot welds. Weld J 83(11):308
87. Behravesh SB, Jahed H, Lambert S (2011) Characterization of magnesium spot welds under tensile and cyclic loadings. Mater Des 32(10):4890–4900
88. Kang J, Chen Y, Sigler D, Carlson B, Wilkinson DS (2015) Fatigue behavior of dissimilar aluminum alloy spot welds. Procedia Eng 114:149–156
89. Pereira A, Ferreira J, Antunes F, Bártolo P (2014) Assessment of the fatigue life of aluminium spot-welded and weld-bonded joints. J Adhes Sci Technol 28(14-15):1432–1450
90. Xiao L, Liu L, Chen DL, Esmaeili S, Zhou Y (2011) Resistance spot weld fatigue behavior and dislocation substructures in two different heats of AZ31 magnesium alloy. Mater Sci Eng A 529:81–87
91. Patel VK, Bhole SD, Chen DL (2014) Fatigue life estimation of ultrasonic spot welded Mg alloy joints. Mater Des 62:124–132
92. Behravesh SB, Jahed H, Lambert S (2014) Fatigue characterization and modeling of AZ31B magnesium alloy spot-welds. Int J Fatigue 64:1–13
93. Hassanifard S, Zehsaz M (2010) The effects of residual stresses on the fatigue life of 5083-O aluminum alloy spot welded joints. Procedia Eng 2(1):1077–1085

94. Lin F, Li TP, Yu Q, Sun LL, Meng QS Diffusion bonding between AZ91 magnesium alloy and 7075 aluminum alloy. In: Advanced Materials Research, 2011. Trans Tech Publ, pp 800–803
95. Balasubramanian V, Ravisankar V, Reddy GM (2008) Effect of postweld aging treatment on fatigue behavior of pulsed current welded AA7075 aluminum alloy joints. J Mater Eng Perform 17(2):224–233
96. Afshari D, Sedighi M, Karimi M, Barsoum Z (2013) On residual stresses in resistance spot-welded aluminum alloy 6061-T6: experimental and numerical analysis. J Mater Eng Perform 22(12): 3612–3619
97. Nodeh IR, Serajzadeh S, Kokabi AH (2008) Simulation of welding residual stresses in resistance spot welding, FE modeling and X-ray verification. J Mater Process Technol 205(1):60–69
98. Long X, Khanna SK (2005) Residual stresses in spot welded new generation aluminium alloys part B–finite element simulation of residual stresses in a spot weld in 5754 aluminium alloy. Sci Technol Weld Join 10(1):88–94
99. Afshari D, Sedighi M, Barsoum Z (2012) Residual stress in resistance spot welded aluminum alloy sheets. i-Manager's J Mech Eng 2(4):6
100. Khanna SK, Long X, Porter WD, Wang H, Liu C, Radovic M, Lara-Curzio E (2005) Residual stresses in spot welded new generation aluminium alloys part A–thermophysical and thermomechanical properties of 6111 and 5754 aluminium alloys. Sci Technol Weld Join 10(1):82–87
101. Emre HE, Kaçar R (2015) Development of weld lobe for resistance spot-welded TRIP800 steel and evaluation of fracture mode of its weldment. Int J Adv Manuf Technol:1–11
102. Jagadeesha T, Jothi TS (2015) Studies on the influence of process parameters on the AISI 316L resistance spot-welded specimens. Int J Adv Manuf Technol:1–16
103. Ashtiani HRR, Zarandooz R (2015) Microstructural and mechanical properties of resistance spot weld of Inconel 625 supper alloy. Int J Adv Manuf Technol:1–13
104. Lang B, Sun D, Li G, Qin X (2008) Effects of welding parameters on microstructure and mechanical properties of resistance spot welded magnesium alloy joints. Sci Technol Weld Join 13(8): 698–704
105. Hou LL, Qiu RF, Shi HX, Guo JQ (2014) Properties of resistance spot welded joint between mild steel and aluminum alloy with an interlayer of AlCu28. Appl Mech Mater 675:15–18
106. Qiu RF, Shi HX, Yu H, Zhang KK, Tu YM, Satonaka S (2010) Effects of electrode force on the characteristic of magnesium alloy joint welded by resistance spot welding with cover plates. Mater Manuf Process 25(11):1304–1308
107. Luo H, Hao C, Zhang J, Gan Z, Chen H, Zhang H (2011) Characteristics of resistance welding magnesium alloys AZ31 and AZ91. Weld J 90:249–257
108. Cao X, Jahazi M, Immarigeon J, Wallace W (2006) A review of laser welding techniques for magnesium alloys. J Mater Process Technol 171(2):188–204
109. Qiu R, Iwamoto C, Satonaka S (2009) The influence of reaction layer on the strength of aluminum/steel joint welded by resistance spot welding. Mater Charact 60(2):156–159
110. Qiu R, Iwamoto C, Satonaka S (2010) Interfacial reaction layer in resistance spot welded joint between aluminium alloy and austenitic stainless steel. Mater Sci Technol 26(2):243–246
111. Qiu R, Satonaka S, Iwamoto C (2009) Effect of interfacial reaction layer continuity on the tensile strength of resistance spot welded joints between aluminum alloy and steels. Mater Des 30(9):3686–3689
112. Qiu R, Iwamoto C, Satonaka S (2009) Interfacial microstructure and strength of steel/aluminum alloy joints welded by resistance spot welding with cover plate. J Mater Process Technol 209(8): 4186–4193
113. Qiu R, Shi H, Zhang K, Tu Y, Iwamoto C, Satonaka S (2010) Interfacial characterization of joint between mild steel and aluminum alloy welded by resistance spot welding. Mater Charact 61(7):684–688
114. Arghavani M, Movahedi M, Kokabi A (2016) Role of zinc layer in resistance spot welding of aluminium to steel. Mater Des 102: 106–114
115. Sun X, Stephens EV, Khaleel MA, Shao H, Kimchi M (2004) Resistance spot welding of aluminum alloy to steel with transition material-from process to performance—part I: experimental study. Weld J 83:188-S
116. Oikawa H, Ohmiya S, Yoshimura T, Saitoh T (1999) Resistance spot welding of steel and aluminium sheet using insert metal sheet. Sci Technol Weld Join 4(2):80–88
117. Oikawa H, Saitoh T (1999) Resistance spot welding of steel and aluminium sheet using insert metal. Weld Int 13(5):349–359
118. Watanabe T, Yanagisawa A, Konu Ma S, Doi Y (2006) Resistance spot welding of mild steel to Al-Mg alloy. Weld Int 20(4):290–294
119. Ibrahim I, Ito R, Kakiuchi T, Uematsu Y, Yun K, Matsuda C (2015) Fatigue behaviour of Al/steel dissimilar resistance spot welds fabricated using Al-Mg interlayer. Sci Technol Weld Join: 1362171815Y. 0000000086
120. Qiu R, Wang N, Shi H, Cui L, Hou L, Zhang K (2015) Joining steel to aluminum alloy by resistance spot welding with a rivet. Int J Mater Res 106(1):60–65
121. Ling Z, Li Y, Luo Z, Feng Y, Wang Z (2016) Resistance element welding of 6061 aluminum alloy to uncoated 22MnMoB boron steel. Mater Manuf Process (just-accepted)
122. Luo AA (2013) 8 - applications: aerospace, automotive and other structural applications of magnesium. In: Pekguleryuz MO, Kainer KU, Kaya AA (eds) Fundamentals of magnesium alloy metallurgy. Woodhead Publishing, pp 266–316
123. Palanivel S, Nelaturu P, Glass B, Mishra R (2015) Friction stir additive manufacturing for high structural performance through microstructural control in an Mg based WE43 alloy. Mater Des 65:934–952
124. Liu L, Ren D, Liu F (2014) A review of dissimilar welding techniques for magnesium alloys to aluminum alloys. Materials 7(5): 3735–3757
125. Luo Y, Li JL (2014) Analysis of nugget formation during resistance spot welding on dissimilar metal sheets of aluminum and magnesium alloys. Metall Mater Trans A 45a(11):5107–5113
126. Zhang Y, Luo Z, Li Y, Liu Z, Huang Z (2015) Microstructure characterization and tensile properties of Mg/Al dissimilar joints manufactured by thermo-compensated resistance spot welding with Zn interlayer. Mater Des 75:166–173
127. Penner P, Liu L, Gerlich A, Zhou Y (2013) Feasibility study of resistance spot welding of dissimilar Al/Mg combinations with Ni based interlayers. Sci Technol Weld Join 18(7):541–550
128. Sun M, Niknejad S, Zhang G, Lee M, Wu L, Zhou Y (2015) Microstructure and mechanical properties of resistance spot welded AZ31/AA5754 using a nickel interlayer. Mater Des 87: 905–913
129. Penner P, Liu L, Gerlich A, Zhou Y (2014) Dissimilar resistance spot welding of aluminum to magnesium with Zn-coated steel interlayers. Weld J 93(6):225s–231s
130. Qiu R, Higuchi K, Satonaka S, Iwamoto C (2009) Characterization of joint between titanium and aluminum alloy welded by resistance spot welding with cover plate. 溶接学会論文集 27 (2):109s–113s
131. Pereira A, Ferreira J, Antunes F, Bártolo P (2010) Analysis of manufacturing parameters on the shear strength of aluminium adhesive single-lap joints. J Mater Process Technol 210(4):610–617
132. Tao W, Ma Y, Chen Y, Li L, Wang M (2014) The influence of adhesive viscosity and elastic modulus on laser spot weld bonding process. Int J Adhes Adhes 51:111–116

133. Liu L, Ren D, Li Y (2011) Static mechanics analyses of different laser weld bonding structures in joining AZ61 Mg alloy. Int J Adhes Adhes 31(7):660–665
134. Shen J, Zhang Y, Lai X, Wang P (2012) Adhesive placement in weld-bonding multiple stacks of steel sheets. Weld J 91:59s–66s
135. Zhang Y, Sun H, Wang P-C, Chen G (2014) Improvement of process robustness in weld bonding of galvanized DP780 steel. Weld J 93(12):472S–481S
136. Sam S, Shome M (2010) Static and fatigue performance of weld bonded dual phase steel sheets. Sci Technol Weld Join 15(3):242–247
137. Khan MF, Dwivedi D, Ghosh P (2010) Studies on the effect of process parameters on the shear performance of joints of aluminium alloy produced by adhesive joining, spot welding and weld-bonding. In: Proceedings of the 36th International MATADOR Conference. Springer, pp 287–292
138. Darwish S (2003) Characteristics of weld-bonded commercial aluminum sheets (BS 1050). Int J Adhes Adhes 23(3):169–176
139. Zheng R, Lin J, Wang P-C, Wu Y (2015) Correlation between surface characteristics and static strength of adhesive-bonded magnesium AZ31B. Int J Adv Manuf Technol:1–10
140. Senkara J, Zhang H (2000) Cracking in spot welding aluminum alloy AA5754. Weld J 79(7):194-s
141. Ghazanfari H, Naderi M (2014) Expulsion characterization in resistance spot welding by means of a hardness mapping technique. Int J Miner Metall Mater 21(9):894–897
142. Yi L, Rui W, Xiaojian X, Yang Z (2015) Expulsion analysis of resistance spot welding on zinc-coated steel by detection of structure-borne acoustic emission signals. Int J Adv Manuf Technol:1–8
143. Qiu R, Wang N, Shi H, Zhang K, Satonaka S (2014) Non-parametric effects on pore formation during resistance spot welding of magnesium alloy. Sci Technol Weld Join 19(3):231–234
144. Tu YM, Qiu RF, Shi HX, Yu H, Zhang KK (2011) Analyses of influencing factors of pore formation during resistance spot welding of magnesium alloy. Mater Process Technol Pts 1-4 291-294:2885–2888
145. Zhang H, Senkara J, Wu X (2002) Suppressing cracking in RSW AA5754 aluminum alloys by mechanical means. ASME J Manuf Sci Eng 124:79–85
146. Lum I, Biro E, Zhou Y, Fukumoto S, Boomer D (2004) Electrode pitting in resistance spot welding of aluminum alloy 5182. Metall Mater Trans A 35(1):217–226
147. Zhou Y, Fukumoto S, Peng J, Ji C, Brown L (2004) Experimental simulation of surface pitting of degraded electrodes in resistance spot welding of aluminium alloys. Mater Sci Technol 20(10):1226–1232
148. Peng J, Fukumoto S, Brown L, Zhou N (2004) Image analysis of electrode degradation in resistance spot welding of aluminium. Sci Technol Weld Join 9(4):331–336